Computational Modeling of Anterior Cruciate Ligament and Meniscus Strain During Stop-Jump Landings

by

Jin Zhu

A thesis
presented to the University of Waterloo
in fulfillment of the
thesis requirement for the degree of
Master's of Applied Science
in
Mechanical Engineering

Waterloo, Ontario, Canada, 2021

Author's Declaration

I hereby declare that I am the sole author of this thesis. This is a true copy of the thesis, including any required final revisions, as accepted by my examiners.

I understand that my thesis may be made electronically available to the public.

Abstract

The anterior cruciate ligament (ACL) is one of the most critical joint stabilizers in the knee. Stop-jump landings are a particularly common maneuver that result ACL injuries due to the large impact forces on the knees combined with forward momentum. The objective of this study was to understand the extent to which certain lower limb kinematic and kinetic parameters contributed to greater ACL and meniscus strains during stop-jump landings. A computational modeling approach was used to simulate this jump landing virtually to allow for analysis of mechanical behavior throughout a 270 ms time window. Available motion capture data from 5 human participants performing a stop-jump landing was used to compute subject-specific muscle forces and 3D kinematic curves in *OpenSim* software. These outputs subsequently drove a virtual simulation of the jump on a finite element (FE) model of the knee joint in Abaqus CAE. The methodology starts with scaling default models in *OpenSim*, followed by computing joint kinematics, muscle forces, and joint moments in the right leg. These values were then grouped into 7 sagittal plane inputs for the FE model. The resulting strains were compared to various sagittal plane kinematic and kinetic parameters through bivariate and multivariate regression analysis to identify which parameters were a significant contributor to increased strain. Understanding and quantifying the effects of these parameters on the ACL and meniscus provided insight that may offer biomechanical recommendations on how to prevent ACL and meniscus injury.

The resulting average peak ACL strain was 7.9±2.4% and 1.01±0.65% for the meniscus. A bivariate correlation study comparing strain with sagittal plane parameters found that there was a strong correlation between ACL strain and the knee range of flexion during the period from ground contact to peak ground reaction force (GRF) time (r=-0.81, p=0.075). No correlation between high quadriceps forces and increased ACL strain was observed despite the common belief that high quadriceps forces often lead to excessive anterior tibial shear. High internal knee extension moments were correlated with increased meniscal strain (r=0.796, p=0.025), which was likely attributed to the high compressive forces applied to the meniscus while the participant was attempting to decelerate the landing. The knee range of landing flexion was found to offer a more accurate prediction of ACL strain compared to instantaneous flexion, as it is not enough to assess the knee flexion only at a certain instance of the landing. It is rather the additional knee flexion after ground contact up until peak GRF that better characterizes a "soft-landing". High quadriceps muscle forces can also protect the ACL by resisting anterior tibial translation when the angulation of the tibia relative to the femur results in posterior tibial shear.

Acknowledgements

I would like to first and foremost thank my supervisor Dr. Naveen Chandrashekar for giving me the opportunity to work on this meaningful project within the University of Waterloo Orthopedic Biomechanics Lab. His guidance and teachings have strengthened my passion for biomechanics and allowed me to significantly develop my research and writing skills.

I am immensely grateful to Harish Rao and Ryan Bakker for not only laying the foundational work to make this project possible, but for also being so thorough and patient with answering my questions and offering their expertise.

Thank you to the members of the Orthopedic Biomechanics Lab for making this experience all the more enjoyable; Shamanth Hampali for his constant optimism, Mayank Kalra for his research advice, and Dan Loewen for his inspiring motivation.

And last but not least, thank you to Edward Poon, my friends, and family for all their endless support.

Table of Contents

List of Figures

List of Tables

Chapter 1

Introduction

1.1 Motivation

The anterior cruciate ligament (ACL) plays a critical role in keeping the knee joint intact, preventing excessive tibial translation and rotation. ACL injuries are a costly burden for not only the patient but also for health care systems, as they are highly prevalent and include many long-term challenges. In North America alone, there can be up to 250 000 ACL-related injuries each year (Griffin et al., 2006). These injuries significantly impact a person's mobility, as the ACL is one of the main knee joint stabilizers, whose functionality is required in daily tasks where any lower limb movement is involved. The meniscus also acts as a vital part of the knee joint, whose biomechanical behavior is even less well understood than the ACL. There has been evidence that damage to either the ACL or the meniscus also leads to further joint cartilage changes over time and increases the risk of developing osteoarthritis (Hall et al., 2016). What is important to note is that the majority of ACL injuries result from non-contact conditions, implying that the ability to reduce the risk of ACL or meniscus tearing can be controlled through conscious execution of safe practices during physical activities. A large body of literature has already contributed towards better understanding the biomechanical nature of ACL strain during activities such as vertical jump landings; however, limited data exists for both the causes of meniscus strain and strain behavior during stop-jump landings. Stop-jump tasks occur more often during ACL injury prevalent sports such as basketball, soccer, and volleyball than vertical jump landings. Therefore there is a great demand for stop-jump related biomechanical recommendations for injury prevention.

With the rise of computational tools available in the biomechanics community, there is

an emerging field of research being done on virtual joint models to visualize and quantify the effects of various mechanical factors on ligaments and cartilage. Up until the completing this thesis, there have been no documentation of a study that combined both the use of *OpenSim*, a biomechanical modeling software, and finite element (FE) modeling to investigate the frame by frame behavior of the ACL and meniscus during a stop-jump landing.

1.2 Objective

The main objective of this study was to understand the range for normal ACL strain during a stop-jump task, which sagittal plane parameters were the main contributors towards increased ACL strain, and how they were interrelated. Parameters that were investigated include kinematic variables, muscle forces, and joint moments. A collection of force plate and motion capture marker data has already been collected from previous experiments carried out by Bakker et al. (2014) from which *OpenSim* was used to compute muscle force values. An FE knee model based on a cadaver knee specimen was also developed and validated by Rao (2020). Therefore the scope of this study was not to focus on the data collection process nor model-building but instead was aimed at correctly applying processed inputs into the FE model and understanding the biomechanical significance of the simulation results regarding strain behavior.

This study also provided an insight into what were the normal ranges of meniscus strain for stop-jump landings tasks. Similar to the ACL strain data, this study has aimed to explain the relationships between certain sagittal plane parameters and meniscus strain. Although there is a richer body of studies related to ACL strain to compare with, the results offered a preliminary understanding of how the meniscus behaves during a stop-jump landing.

Chapter 2

Background

2.1 Knee Anatomy and Injury Factors

To establish a common nomenclature for ease of communication, a collection of anatomical terms are used conventionally when referring to various anatomical positioning and locations. The next section will briefly explain the relevant knee anatomy and spatial terminology required to better understand the factors that contribute to ACL and meniscus strain.

2.1.1 Anatomical Terms

There are three reference planes used as a basis for describing the human body's movements, which intersect at the center of the body as shown in Figure 2.1. The frontal plane spans between the left and right side of the body, which is perpendicular to the sagittal plane that is aligned with the body's axis of symmetry. The third plane is the transverse plane, which separates the body into a top and bottom section.

When describing location or direction on a human body, the point of reference is also taken at the center of the body, which is illustrated in Figure 2.2. Anterior and posterior directions represent the forward and backward directions from the frontal plane, while the superior and inferior directions point towards the head or the feet respectively. The lateral direction points away from the sagittal plane while the medial direction points closer to the sagittal plane, no matter if the point of interest is on the left or right side of the body.

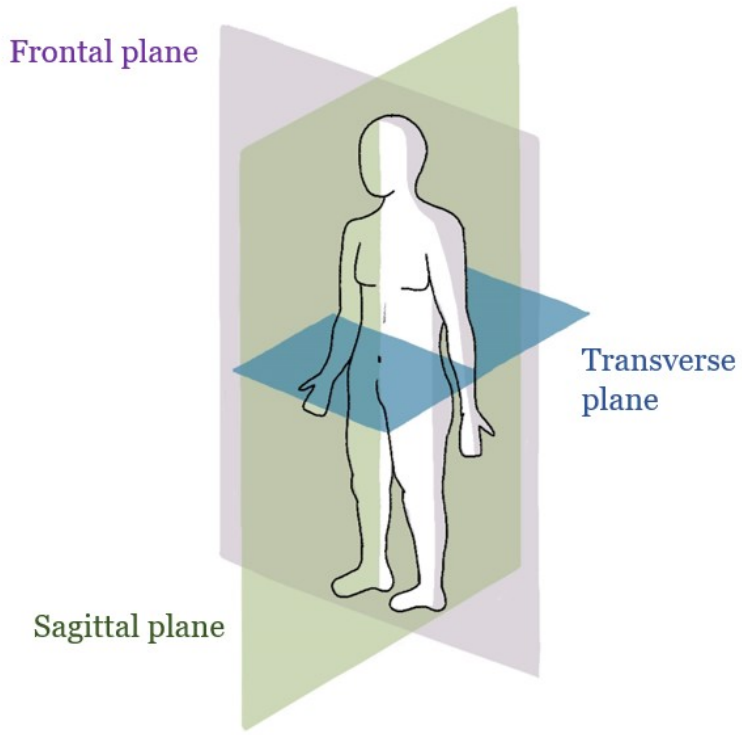

Figure 2.1: Anatomical planes

Proximal and distal also represent directions farther and closer to the center of the body respectively.

The main motions exhibited by the lower limbs can be grouped into flexion-extension, adduction-abduction, and internal and external rotations. Flexion is the term for what is commonly referred to as "bending", while extending refers to the return to neutral anatomic position, as shown in Figure 2.3. Adduction-abduction movements occur in the frontal plane, where adduction refers to moving toward the body's midline. Internal and external rotations occur about the transverse plane, with external rotation turning away from the center of the body.

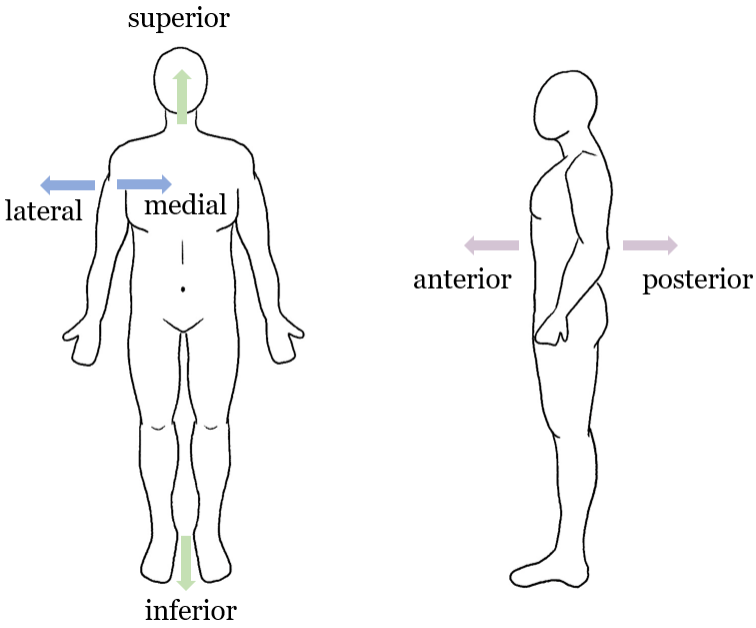

Figure 2.2: Anatomical terms for directions

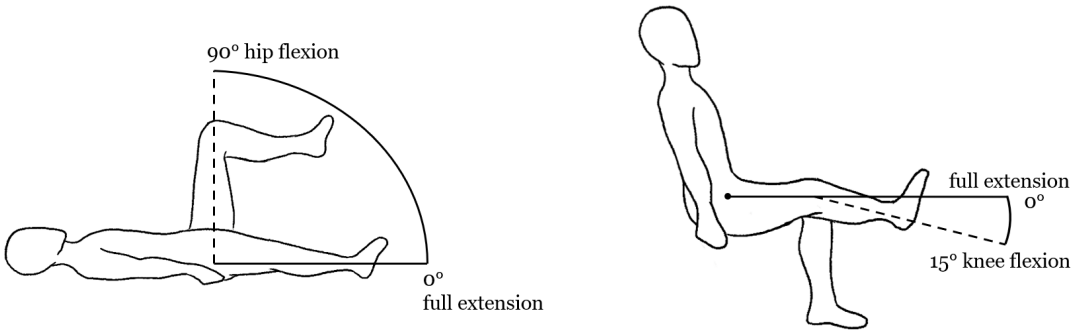

Figure 2.3: Hip and knee motions.

2.1.2 Knee Anatomy

The musculoskeletal components that make up the knee joint can be categorized into three main groups: the bones, the ligaments, and the cartilage, as represented in Figure 2.4.

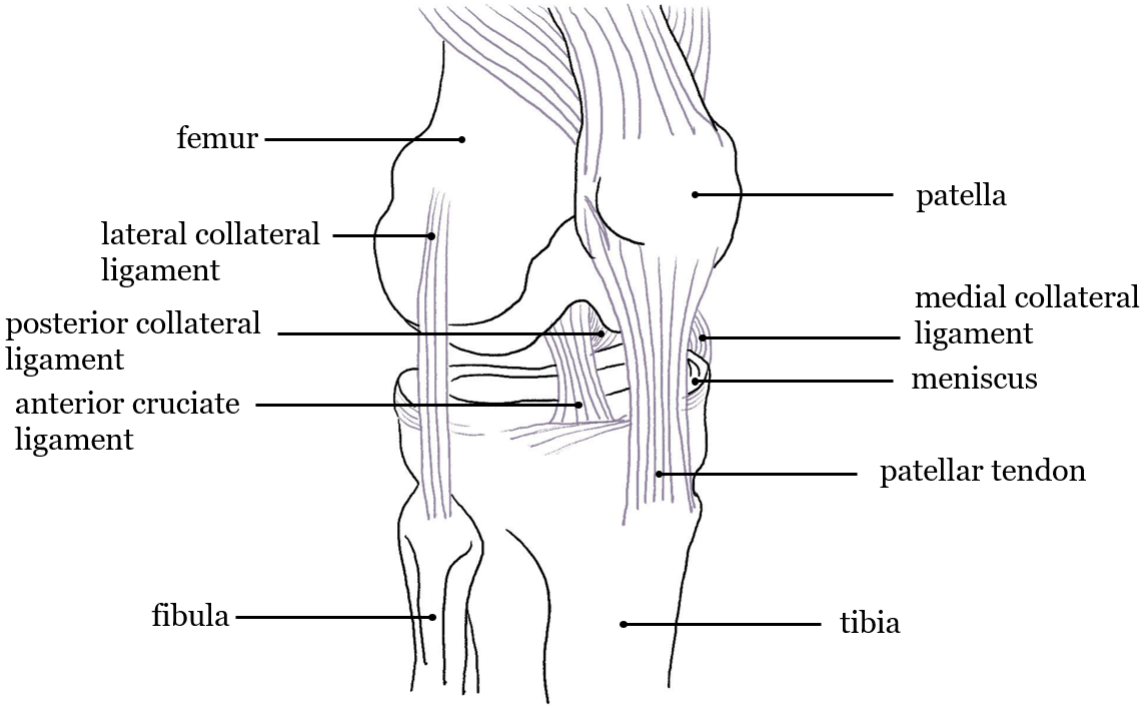

Figure 2.4: Knee anatomy. Adapted from Bakker (2014)

The bones consist of the femur, tibia, fibula, and patella. The knee contains two joint interfaces despite being commonly thought of as one joint. The patella-femoral joint is responsible for acting as an additional length of moment arm for the quadriceps muscles, and facilitates knee extension moments induced by the quadriceps' contraction. The patella acts as a lever that allows tensile forces from the quadriceps to pull on the tibia. The tibia-femoral joint supports axial loads experienced as a result of ground reaction forces (GRF) and absorbs the impact for activities such as walking, running, and jumping.

There are four major ligament groups that help secure the knee joint together: two cruciate ligaments that criss-cross between the femur and tibia, and two collateral ligaments which span the medial and lateral sides of the knee. The anterior and posterior ligaments (ACL and PCL) prevent the tibia from translating anteriorly and posteriorly relative to

the femur, as well as resisting internal tibial rotation (Noyes, 2009). The medial and lateral collateral ligaments (MCL and LCL) wrap along the sides of the knee joint and also help with preventing excessive tibial translation in all transverse plane directions. With the MCL wider than the LCL, both also resist valgus and varus motions, which is when the knee bends inwards and outwards within the frontal plane.

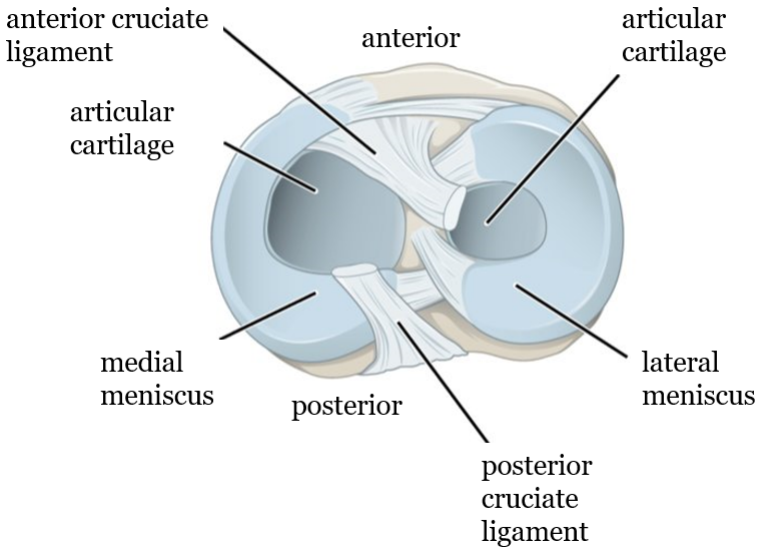

Figure 2.5: Knee ligaments. Adapted from Kean et al. (2017)

The cartilaginous components of the knee joint consists mainly of the medial and lateral meniscus. These crescent shaped disks are important for absorbing shock during high-impact activities. Due to the flexible cartilage material, they serve to minimize spikes in contact stresses during joint movement.

There are a great number of muscles that articulate with the knee joint and they can be grouped into three main actuator groups shown in Figure 2.6: the quadriceps, the hamstrings, and the calf muscles. The quadriceps muscles includes the rectus femoris and the three vastus muscles (vastus intermedius, lateralis, and medialis (Moore & Dalley, 1999)). These muscles are responsible for extending the knee by creating tensile forces on the tibia via the patellar tendon.

As antagonists to the quadriceps muscles, hamstrings act as the main knee flexors and consists of the bicep femoris long head, bicep femoris short head, semitendinosus, and semimembranosus (Moore & Dalley, 1999). Furthermore these muscles also attach to the

pelvis (with the exception of the bicep femoris short head), meaning they will also extend the hip.

The two gastrocnemius muscles (lateral and medial) and the soleus muscle make up the calf muscles. However the soleus does not insert into the femur unlike the two gastrocnemius muscles, therefore it does not articulate directly with the knee. Instead, the soleus connects from the tibia to the calcaneus bone in the foot, contributing ankle plantar flexion. The gastrocnemius muscles also attach to the calcaneus, but originate at the femur, thereby contributing to knee flexion.

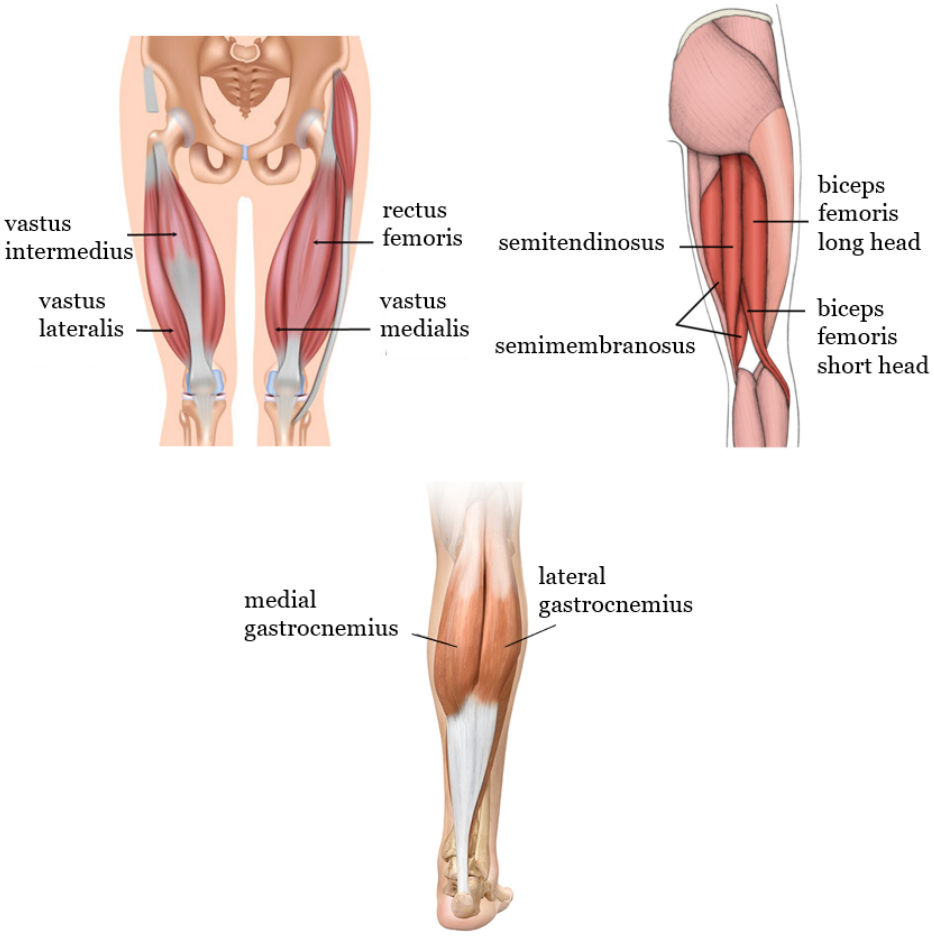

Figure 2.6: Knee muscles. Adapted from *Your Health Guideline* (2019), *Sports Injury Bulletin* (2018), and *Fairview Health Services* (2000).

2.2 Strain Injuries in Stop-Jump Tasks

Many of the knee joint injuries in physical activities are a result of attempting to stabilize high impact forces. Jump landings are one of the most common examples of where muscles, ligaments, and cartilaginous components in the knee joint must collectively resist high inertial effects. As the ACL acts as one of the main knee stabilizers, several studies have shown that landings exerting excessive forces and torques on the knee joint create a high risk for ACL tearing (Bakker, 2014; Cerulli et al., 2003; Chandrashekar et al., 2005; Chappell et al., 2007; Peebles et al., 2020; Yu et al., 2006). The two most common types of landing tasks are vertical-jump landings and stop-jump landings (Peebles et al., 2020). The difference between the two forms of landings is that the vertical-jump landing occurs when the person is falling vertically from the jump, while a stop-jump occurs when the person takes a leap forward followed immediately by a change in direction. This change of direction is usually in the vertical direction, transitioning into a vertical-jump, but can also be a full stop. Both landings can take the form of two-leg or single-leg landings (depicted in Figure 2.7), keeping in mind that the knee would bear more load in a one-footed landing. In experimental studies, vertical-jumps are usually replicated by either jumping off a platform of a certain height onto the force plate (Peebles et al., 2020), or by asking the participant to jump as high as possible from the force plate (Bakker, 2014). Stop-jumps studies will often ask participants to take a running approach (Yu et al., 2006) or a few strides before landing on the force plate and taking-off vertically or simply holding a stabilized stationary pose (Kar & Quesada, 2012).

It is understood that both types of jump landings require the ACL and meniscus to withstand moderate to high magnitudes of shock to stabilize the activity. However there is a significantly larger body of literature studying vertical-jump tasks compared to stop-jump tasks. Stop-jump tasks are frequently associated with ACL injuries in numerous athletic activities including basketball (Krosshaug et al., 2007), soccer (Gomes et al., 2008), volleyball (Dai et al., 2019), and many more. There is currently a lack of consistent understanding of stop-jump-specific injury mechanics. The clear difference in inertial patterns from stop-jumps compared to vertical-jumps merits further investigation into how ACL and meniscus injuries can be prevented during stop-jump tasks in particular.

A limited collection of experimental studies have begun to offer more insights into what conditions encourage the risk of ACL damage in recent years (Peel et al., 2021; Yu et al., 2006; Kar & Quesada, 2012; Peebles et al., 2020). Yu et al. (2006) reported that the rotational flexion velocity at the hip and knee during ground contact were negatively correlated with the maximum GRF, both in the posterior and vertical direction. Their study also reported that with greater posterior and vertical GRF, high knee extension

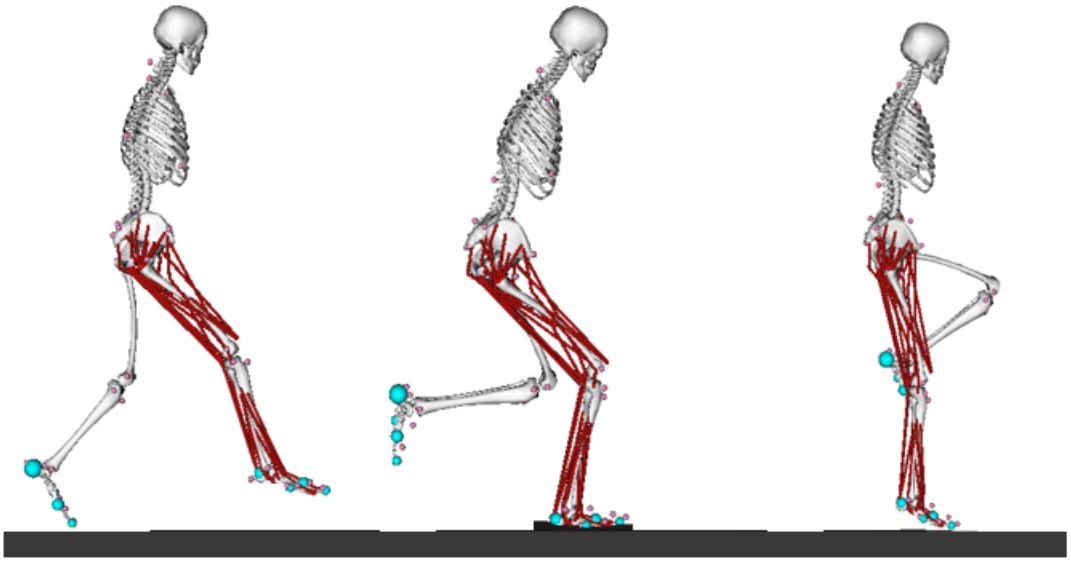

Figure 2.7: Example of single-leg stop-jump landing.

moments and tibial anterior shear force was observed as well. Peel et al. (2021) found that increased quadriceps muscle forces, particularly the vastus lateralis, contributed highly to greater ACL loads for a stop-jump task from an all-female participant sample. Kar and Quesada (2012) also studied ACL loading among an all-female group and also observed that the tibial shear force was directed anteriorly during their entire trials, and also reported increased activation in the rectus femoris, vastus lateralis, and bicep femoris muscles in sync with peak ACL strain periods. Differences in stop-jump landing mechanics among males and females was also investigated (Peebles et al., 2020), supporting the theory that females are at a greater risk of suffering ACL damage, as the females of the sample exhibited higher knee abduction angles, internal knee adduction moments and lesser knee extension moments compared to the males. Regardless of sex-based differences, higher posterior GRF and knee adduction moments were observed in stop-jump tasks compared to vertical-jump tasks, which suggests that stop-jump tasks may be a higher risk maneuver in terms of ACL damage. This highlights the importance of determining injury-mitigating recommendations for a stop-jump task.

Both the studies by Yu et al. (2006) and Peebles et al. (2020) were carried out using 3D marker data of anatomical landmarks placed on each participant along with force plate data

to obtain GRFs. Other studies such as Dai et al. (2019) used mainly electromyography (EMG) data to evaluate the effects of various muscle forces on the risk of ACL injury. Some studies even used video analysis to evaluate the kinematic patterns that lead to ACL damage from footage of real-life sporting injuries. Krosshaug et al. (2007) analyzed a collection of 39 clips of ACL injury cases observed in basketball, of which 22 were female athletes. The most frequent action that resulted in injury for males was single-leg landings and 2-leg landings for females. Whether they were vertical-jump or stop-jump landings was not distinguished. This study found that the females had much higher knee and hip flexion angles during injury, contrary to the commonly reported conclusion that females exhibit more extension during landings. Injuries also occurred on average 33 ms to 39 ms after ground contact across all cases. Although muscle force analysis was outside the scope of their study, Krosshaug et al. points out that the higher flexion observed in the female cases combined with other observations conflicting with the literature, the relationship between strain, flexion angle, quadriceps forces, and GRF is still ambiguous.

2.3 Computational Tools

The use of motion capture systems, force plates, and EMG sensors remain the most commonly used data collection tools within biomechanics studies. However exclusively analyzing marker and force plate data does not provide direct information on the contraction forces of individual muscle groups. Even with EMG sensors, which can only provide excitation levels of one muscle group per sensor, there is a limited number of muscles one can analyze at once. It is also challenging to compare EMG data between independent studies and draw meaningful conclusions from values that are heavily dependant on the experimental setup and post-processing methodology. Computational approaches allow evaluation of numerous kinematic and kinetic parameters at once, and offer the ability to identify relationships within internal components of a complex musculoskeletal system. With the rise of advancements in computational biomechanics, new opportunities for quantifying the nature of ACL and meniscus injury become increasingly available.

2.3.1 *OpenSim*

OpenSim is an open-source multibody dynamic modeling software used for biomechanical applications and was developed by Stanford University (Delp et al., 2007). The program allows one to simulate motions on a virtual musculoskeletal model by inputting kinematic marker trajectories from motion capture as well as GRF data. Built-in functions can scale

the model to custom anatomical proportions and then compute kinematic and inertial values such as joint angles, joint reaction forces, and muscle forces. Muscle force curves can also be inputted into the model to run a predictive simulation for the resulting motion. *OpenSim* has been used for numerous dynamic loading scenarios such as jump landings (Bakker, 2014), athletic performance optimization (Hamner et al., 2010), surgical outcomes (Li et al., 2019), and even animal biomechanics (Becker et al., 2019).

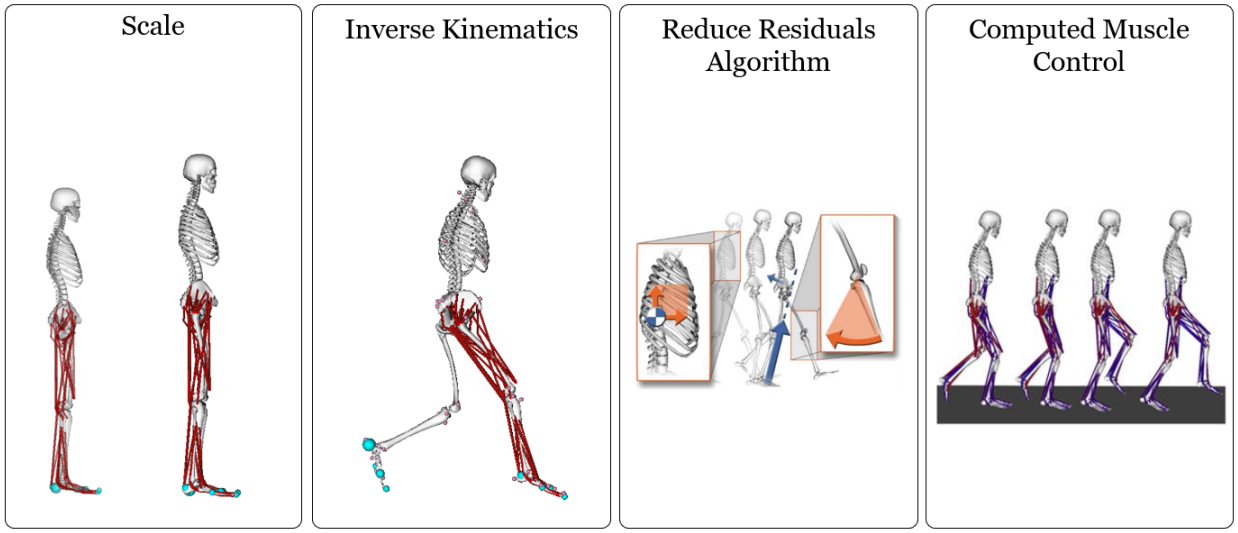

Figure 2.8: OpenSim Workflow. Adapted from SimTK.

As depicted in Figure 2.8, a typical *OpenSim* workflow begins by scaling the model, performing inverse kinematics analysis, reducing the residuals, and using the Computed Muscle Control (CMC) function to obtain muscle forces values. Generic *OpenSim* models are available with the default download package, which can be modified and scaled. During the Scale function, which is usually performed to customize the base model, the software attempts to match the location of landmarks on the model to the marker locations input from the experimental motion capture data (Delp et al., 2007). This is typically done by inputting a few frames of marker data where the participant is stationary.

The Inverse Kinematics function typically follows the Scale step where the software attempts to fit the marker trajectories of the whole experimental input motion to the range of motion possible in the model (Delp et al., 2007). The objective function of this algorithm is to minimize the deviation from the experimental trajectories to the resultant

virtual trajectories as much as possible using a weighted least-squares approach. This step is where the joint angles are computed as well.

Before solving for muscle force values using the CMC function, a priming step called the Residual Reduction Algorithm (RRA) is usually performed to optimize the accuracy of CMC results. When attempting to balance out the inertial components of the system, such as external body accelerations, internal joint moments, and GRF, it is impossible to solve every frame without some residual values. The RRA step attempts to minimize these residuals by adjusting the torso's center of mass location. The user also has the flexibility to adjust the stringency of minimizing the degree of kinematic deviation and the limit on residual forces, which are opposing factors.

Once the RRA step is completed, the model is ready for muscle force computation. The CMC algorithm in *OpenSim* calculates individual muscle activation in 10 ms increments, where it will solve for the best muscle force set to satisfy the motion at the end of each increment (Delp et al., 2007). The residual forces and moments along with the amount of kinematic deviation resulting after the CMC step is often used to determine how accurate the simulation is (J. L. Hicks et al., 2015).

Both studies by Peel et al.(2021) and Kar and Quesada (2012) studied ACL loading using *OpenSim*. The former computed the tensile force applied to the ACL based on the sagittal plane knee joint reaction force calculations. Using muscle forces and joint angles computed in *OpenSim*, they were able to isolate the muscle contributions to knee joint reaction forces for 80 muscle actuators across their entire model. Kar and Quesada (2012) were able to model the ACL in *OpenSim* as a non-linearly elastic passive tissue that attaches from the anterior region of the tibia to between the femoral condyles. The anteromedial and posterolateral bundles were grouped as one. A strain limit of 15% had to be defined and a stiffness of 240 N/mm was assigned. The limitation with this ACL model is that the knee joint is simplified to only having bones, muscles, and the ACL ligament alone. There are menisci and ligaments definitions missing from this model, as well as no contact conditions between the interfaces of the knee joint. *OpenSim* is well suited for macro-studies of motion, joint forces, and obtaining many muscle force values at once. However, to more accurately represent the complex sub-components and interactions of the knee joint cartilage and ligaments, a much more detailed model is required.

2.3.2 Finite Element Knee Modeling

Finite element (FE) analysis offers a powerful predictive tool that is well suited for a system with as complex geometrical and material properties as the knee joint. Brekelmans et al.

(1972) marks one of the earliest studies that used FE methods on orthopedic mechanics, starting by applying loads to a 2D femur. Since then, several studies have attempted develop increasingly detailed FE models, particularly of the knee (Guo et al., 2009; Rao, 2020; Polak, 2018; A. Kiapour et al., 2014). Some studies have produced knee models from healthy participants using computed tomography (CT) scans to understand stress distributions in the knee joint during ground contact of normal gait cycles (Guo et al., 2009). Others have obtained both CT and magnetic resonance imagining (MRI) scans from cadaveric knee specimens to simulate vertical-jump landings (Rao, 2020). Even an FE model of the entire body is available, developed by the Global Human Body Models Consortium (GHBMC) (Schwartz et al., 2015).

The availability of validated knee models is particularly valuable for better understanding of ligament behavior. Kiapour et al. (2014) was able to validate the kinematics, strain values, and cartilage pressure of their *in-vitro* knee simulator using cadaveric experiments. Their dynamic cadaveric testing consisted of dropping half the subject's bodyweight onto the foot to simulate a vertical-jump landing. The resulting peak ACL strain was found to be 5.2% from the FE simulation and 7.1% when simulated again with an added anterior shear force of 134 N.

A study by Polak (2018) used the right lower limb component of GHBMC collection of models to simulate ACL strain from two participant vertical-jump landings to obtain an average peak strain value of 4.4%. Rao (2020) would later develop a different subject specific knee model with similar inputs to obtain an average peak strain of 5.4%. Rao was also able to validate their knee model by comparing strain values to cadaveric studies carried out by Bakker (2014).

FE analysis also allows one to quantify the stresses and pressures experienced by the menisci. Guo et al. (2009) found that the medial meniscus experiences greater impact force than the lateral side during normal gait. In addition, the pressure experienced by the medial meniscus exhibited much greater variation than the lateral meniscus, with peak pressures occurring at roughly 45% of the cycle. The peak contact pressure observed in the medial meniscus was 21 MPa, which was consistent with the 22 MPa value found by another FE study (Godest et al., 2002).

Up until this current study, there have been no experiments reported in literature that analyzed ACL and meniscus strains during a stop-jump landing using validated FE methods. Therefore, having established that stop-jumps can be a high-risk maneuver for the knee joint if not exhibiting the correct landing pose, this study combines and applies the benefits of *OpenSim* and FE modeling towards developing a clearer understanding of which factors are significant contributors to causing ACL and meniscus injury.

2.4 Precursor Studies

Many facets of this thesis build upon on the data, testing and validation from previous works. This study offers novel findings regarding the biomechanics of the meniscus and ACL ligament with an emphasis on data processing methods and computational simulation setup rather than data collection and model building. Therefore the next few sections describe how the data, models, and experimental processes were obtained for prior applications in order to understand the rationale behind the methodology of this current study.

2.4.1 Motion Capture Data and *OpenSim*

The kinematic inputs for this current study originates from a collection of data recorded by Bakker (2014) during their study on the effects of sagittal plane biomechanics on the right knee joint during a single-leg vertical-jump landing. Motion capture marker trajectories and force plate sensor data were recorded for both vertical-jump landings *and* stop-jump landing trials from the same set of 10 participants, the latter of which was reserved for this study. Participants were asked to perform both types of maneuvers across an AMTI force plate (OR6-7-2000, AMTI, Watertown, MA) recording their GRFs and moments at a frame rate of 1600 Hz. Simultaneously, the 3D trajectories of 39 digitized markers placed on palpations across the left and right sides of the body are captured at 80 Hz using the *Optotrack* motion capture system (Northern Digital, Waterloo, ON). The *NDI First Principles* software was used to record the force plate and marker data simultaneously, and saved as *C3D* files.

Each trial recording lasted for 5 s, beginning with the participant out of the frame and off the force plate. Once the recording began, participants were instructed to perform the stop-jump across the force plate using their right leg for both the first and second landings. The trial was completed with the right leg still on the force plate area at the end of the second landing, and held still in a single-leg stance for roughly 2 s before the recording stopped. The purpose of maintaining this stationary pose in final few frames of each trial was to serve as a static calibration for subsequent scaling steps in *OpenSim*.

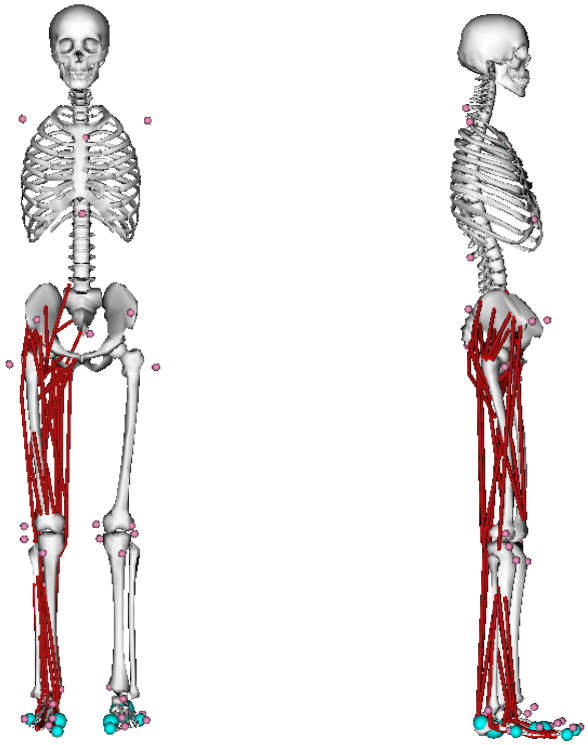

Figure 2.9: *OpenSim* model with motion capture markers and stripped left leg

Each participant's custom *OpenSim* model was scaled to their respective anatomical proportions from a base model developed by Bakker (2014). This model was a modified version of the generic model Gait2392 provided by *OpenSim*, shown in Figure 2.9. Modifications include doubling the maximum achievable isometric contraction for each of the lower limb muscles due to the generic model being designed for low impact activities such as normal gait. As this study was only interested in the right leg biomechanics, muscle components in the trunk and left leg were also removed from the Gait2392 model and replaced with torque actuators to reduce simulation time. This was done with the knowledge that removing these muscles did not affect the computation of right leg muscles forces as the local net torque of individual body segments and joints remained unchanged. Further methodology and justification details behind this step were documented in the work of Bakker (2014).

2.4.2 Dynamic Knee Simulator

Many aspects of the FE model and simulation setup applied in this study were based on previous *in-vitro* experiments. Cassidy et al. (2009) developed one of the early iterations of the University of Waterloo dynamic knee simulator (DKS) which was designed to replicate a jump landing on a cadaver knee specimen. This simulator design was able to offer a more anatomically representative jump simulation compared to previous knee simulators designed by research groups at the University of Michigan (Withrow et al., 2006; McLean et al., 2011), Ohio State University (A. M. Kiapour et al., 2014), and Texas Tech University (Hashemi et al., 2010). The University of Waterloo DKS was able to input dynamic kinematics and muscle forces over time, while the previous simulators could only input instantaneous loads. Bakker (Bakker, 2014) was later able to obtain muscle forces from *OpenSim*, in addition to the motion capture marker trajectories, to reproduce the entire span of a jump landing.

The University of Waterloo DKS intook the relative kinematics for the hip and ankle, with one metal cable actuator for each muscle force group applied by electromechanical actuators. The muscle forces were consolidated into three groups; the quadriceps, hamstrings and calf gastrocnemius muscle forces. The third type of input was a hip extension moment created by pulling posteriorly at a small distance offset from the hip attachment point. Therefore the DKS was driven by these six inputs.

Figure 2.10 shows the setup of these six inputs and how they were exerted on the knee specimen. The hip attachment was installed in a vertical linear actuator while the ankle was likewise fixed onto a horizontal linear actuator. Hence the relative vertical and horizontal kinematic trajectory was computed for the hip and ankle respectively. The actuators for the quadriceps, hamstrings, gastrocnemius muscles, and hip moment were fixed onto the specimen and exerted in directions that simulate the muscle fiber contraction directions. Bakker (2014) was able to collect motion capture data which drove the ankle and hip kinematics, as well as computed the muscle force values from *OpenSim* using GRFs measured from force plates.

The soleus muscle was not included as a DKS input, despite being a major calf muscle. There has been evidence that the soleus plays a non-trivial role in ACL strain behavior (Elias et al., 2003), and this was a limitation of the DKS that this study aimed to improve upon, as the soleus has been included in the stop-jump simulations discussed in this thesis.

Understanding the mechanics of the DKS was important for recognizing the rationale behind the methodology applied in this study. The FE knee model, on which the simulations of this project was computed, was adapted from the FE knee model developed by Rao

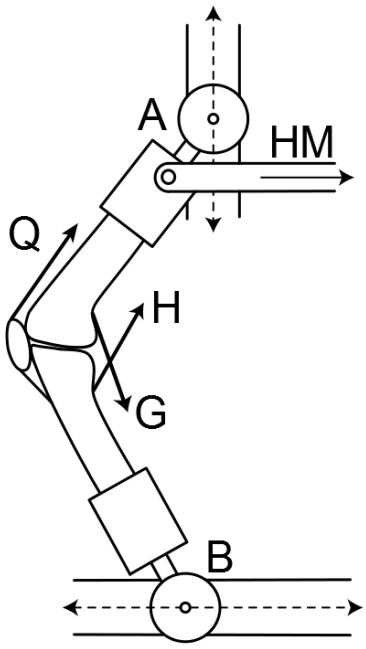

Figure 2.10: Representation of the University of Waterloo DKS. A: hip actuator. B: ankle actuator. Q, H, G: quadriceps, hamstrings, gastrocnemius muscle force cables. HM: hip moment. Schematic adapted from Bakker (2014).

(2020), who based the FE knee model off of the University of Waterloo DKS. Therefore many of the model constraints and prescribed conditions originate from the DKS design.

2.4.3 Finite Element Knee Model Origins

Rao (2020) developed a subject-specific FE knee model from a cadaver originating from a 49 year-old male, which closely represented a 50th percentile U.S. male (Gayzik et al., 2011). A series of steps were involved to develop the model including image processing, meshing, digitizing, and assigning anatomical properties.

The process began with obtaining computed tomography (CT) and magnetic resonance imaging (MRI) scans of the cadaver knee specimen, which were collected at Sunnybrook Medical Center, Toronto, ON, Canada. Once the images of the knee were obtained, a combination of automatic and manual segmentation steps were carried out in an open source software called *3D Slicer*. This process identified different regions and contours of

an image based on pixel characteristics of the CT scans and consolidated the slices into a 3D model, as shown in Figure 2.11. The segmentation results were then post-processed in *SolidWorks* (Dassault Systèmes, Johnston, RI) for smoothing.

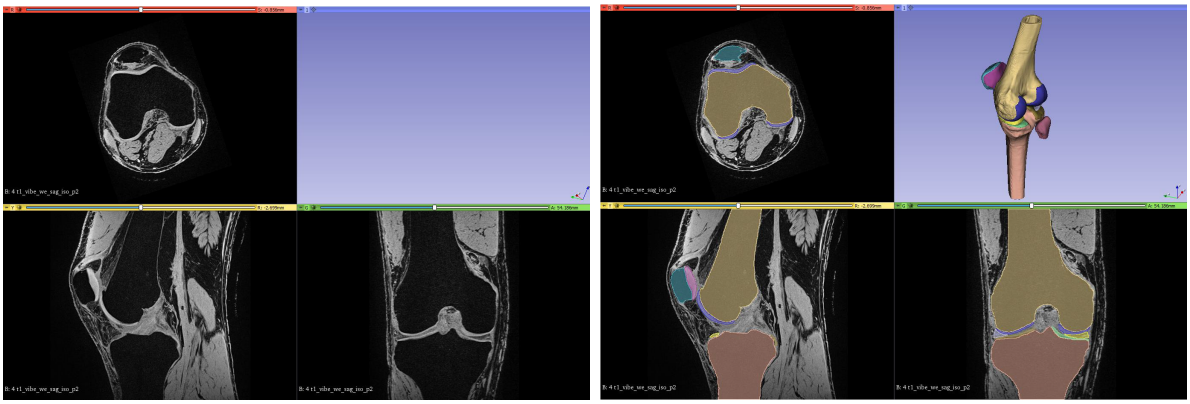

Figure 2.11: MRI images imported into *3D Slicer* (left). Segmentation results with the resulting model (right). Images adapted from Rao (2020).

To later identify the correct placement of ligaments attachment sites in the FE model, a coordinate measuring device was used to digitize anatomical landmarks in the knee. The internal surfaces of the knee joint were first exposed by cutting at the mid-lengths of the cruciate and collateral ligaments. Next, bony landmarks were identified and used as references for the ligament attachment sites. A coordinate measuring device was used to probe and register locations of ligament attachment sites relative to the bony landmarks. The registered bony landmark points were then matched to the model in *3D Slicer*, along with the ligament attachment points, and them imported into *Abaqus CAE* 2018 (Dassault Systèmes, Johnston, RI), the FE software package chosen for the study. Ligaments for which insertion sites were registered include the ACL, the PCL, the MCL, and the LCL.

Bones were modeled using tetrahedral elements and defined as rigid bodies using *HyperMesh* (Altair, Troy, MI) while soft tissue components such as the menisci and other cartilaginous components were modeled with hexahedral elements using *IA-FEMesh* (The University of Iowa, Iowa City, IA) and *MATLAB* (MathWorks, Natick, MA). Cartilaginous components such as the patellar, femoral, and tibial cartilage were fixed to their corresponding bone components such as the patella, femur and tibia via TIE constraints in *Abaqus* so that there was zero relative motion. The surfaces between interfacing joint surfaces, such as the femoral condyles and the menisci, were modeled as frictionless to represent an ideal well-lubricated knee joint capsule.

The values in Table 2.1 summarize the mechanical properties of the various components which make up the knee joint model. All of the bone, cartilage, and menisci materials were defined as isotropic and linearly elastic.

Table 2.1: FE knee model mechanical properties

Knee Joint Component	Deformity	Young's modulus (MPa)	Poisson's ratio
Femur Tibia Patella Fibula	Rigid	8000	0.3
Femoral cartilage Lateral tibial cartilage Medial tibial cartilage	Deformable	20	0.45
Lateral meniscus Medial meniscus	Deformable	59	0.49

The ligaments were modeled as non-linear spring elements as *Abaqus*' non-linear axial connector element. Stiffness values for all ligaments except for the ACL was obtained from Blankevoort et al. (1991). The stiffness values for the PCL, MCL, and LCL bundles were each 9000 MPa, 2750 MPa, and 2000 MPa for each bundle respectively. The ACL stiffness parameter was instead obtained from Chandrashekar et al. (2005), where a non-linear curve was used to define the stiffness, whose linear elastic region was roughly 381 MPa for both ACL bundles combined. This was divided evenly among the anteromedial ACL (AMACL) and posterolateral ACL (PLACL) bundles which act as parallel non-linear springs.

With this model, Rao (2020) simulated single-leg vertical-jump landings from 10 different participants trials, the same participant data used in Bakker (2014) to drive the DKS. The input of forces and kinematics were set up similarly to the DKS experiments performed on the University of Waterloo DKS (Bakker, 2014; Polak, 2018), as represented in Figure 2.12. Like the DKS, the hip was constrained to translate only in the vertical Y direction while rotating about the Z direction to execute the hip moment input. The ankle node was free to translate in the X direction only and was free to rotate about the Z axis and also the X axis, as this was how the DKS was designed.

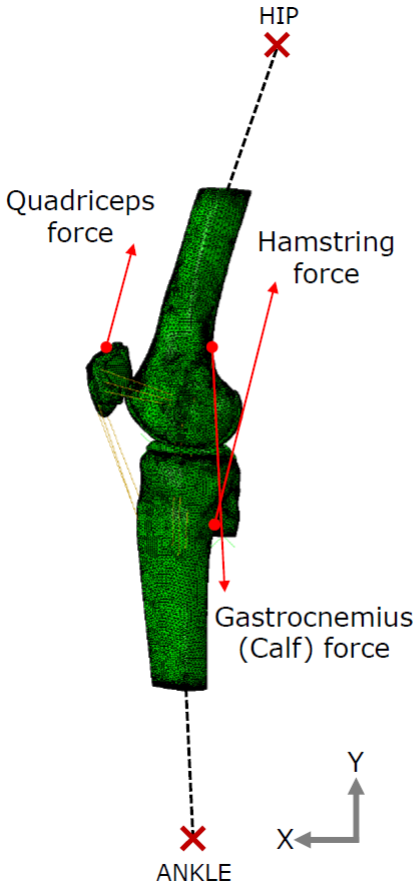

Figure 2.12: Orientations and point of applications in the FE knee model. Adapted from Rao (2020).

The cadaver knee specimen on which the FE knee model was based was also used for experimental vertical-jump landing trials on the DKS (Polak, 2018), simulating 2 of the 10 participant jumps from Bakker (2014). This allowed for validation of the FE model using *in-vitro* testing on the same knee specimen. All jump landing trials were completed before cutting the knee joint ligaments for digitization. Of the two participant trials simulated by Polak (2018), one of them agreed well with the computational ACL strain results simulating half muscle force jumps. The meniscus strains between the experimental and computational half force jumps also agreed well with each other for half muscle force trials. The cadaver specimen unfortunately failed during full muscle force trials, so no comparisons were made between experimental and FE strain results.

As mentioned, Rao (2020) also simulated 10 vertical-jump landing trials on the subject-specific FE knee model, for which the kinematics and the kinetics were the same ones used by Bakker (2014) during their DKS experiments. From these trials, a mean peak ACL strain of 5.4% ±2.6 and mean meniscal strain of 2.3% ± 1.6 was obtained, and agreed well with the mean strain values and trends observed in Bakker's (2014) studies.

Further specifications on how the FE knee model was developed can be found in Rao's study (2020). Only a high-level comprehension of the FE knee model properties is required to understand this current study, as the simulations carried out in this project focused on the application of the model. Being familiar with the *OpenSim* data collection process, the DKS design, and an overview of the FE knee model development will clarify the rationale behind many of the boundary conditions, constraints and input methodology applied in this study.

Chapter 3

Methodology

The methodology can be broken down into four major phases. The first phase involves processing the raw motion capture and force plate data into inputs that were compatible with *OpenSim*. Once the *OpenSim* inputs were prepared, the joint kinematics and muscle forces and moments were computed. These forces and moments were then scaled to the subject-specific FE model and consolidated into the muscle and moment group drivers of the FE simulation. Following the preparation of FE inputs, boundary conditions were established to simulate the stop-jump landing and the results underwent statistical analysis to understand relationships between sagittal plane parameters and strain. The methodology workflow is represented below in Figure 3.1.

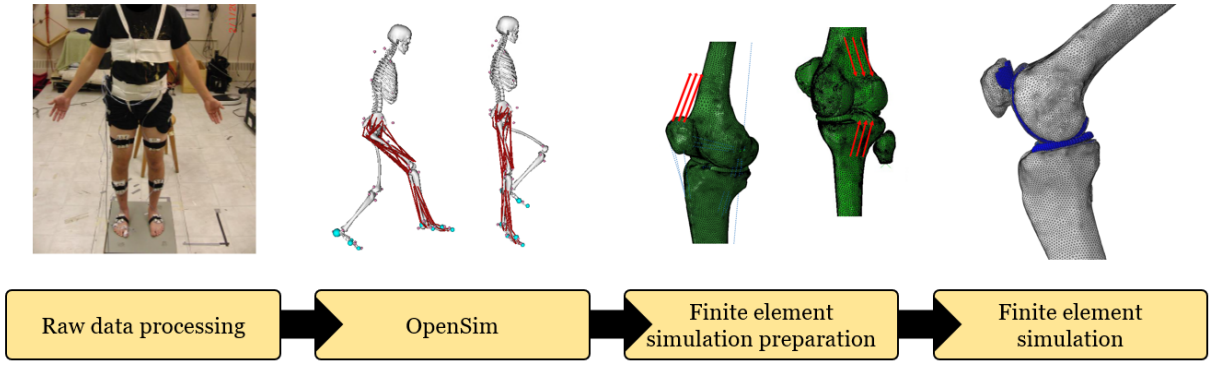

Figure 3.1: Methodology workflow

3.1 Motion Capture and Force Plate Processing

As mentioned in section 2.4.1, a collection of previously recorded raw data files for the motion capture kinematics and the force plate data of each participant was available. These files were initially outputted as *C3D* file formats. During the recording of the 39 marker trajectories, there were instances where the camera did not register the location of individual markers. This occurred as a result of certain markers being obscured or moved momentarily out of the frame. These momentary gaps of visibility led to marker dropout in the kinematic data, which can be observed in the marker trajectory curves within the C3D software, *Visual 3D* (C-Motion, Germantown, MD). Although five or more jump trials were recorded for each participant, the trial with the least amount of marker dropout was selected for the study. Ultimately, out of the original 10 participants from Bakker's study (2014), the data from 5 participants were deemed to have sufficiently minimal marker dropout to be used in this study. This selection process was conducted after a function in *Visual 3D* attempted to fill gaps of data using its built-in interpolation methods. The other 5 discarded participants' stop-jump trials from Bakker's study had marker gaps that were too large to interpolate and would have resulted in excessive residual errors and inaccurate muscle forces during the subsequent *OpenSim* steps. The 5 chosen participants are presented in Table 3.1 below with their anatomical and jump specifications.

Table 3.1: Study participants

	P1	P2	P3	P4	P5
Sex	F	M	M	F	F
Body Mass (kg)	59	72	79	65	66
Femur Length (mm)	399	429	422	404	437
Tibia Length (mm)	368	396	391	381	404
Peak vertical GRF (N)	1198	1655	1823	1816	1287
Landing to Peak GRF Time (ms)	221	201	153	149	219

A few data preparation steps were required to convert the raw data output from the force plate and marker cameras into a file format that was readable by *OpenSim*. The output data format from the force plate sensors were in voltages and were converted to Newton units using a calibration matrix for type 2 force plate sensors provided by the manufacturer. A processing script was written in *MATLAB* to calibrate, transform, filter and format each participant's raw data.

The coordinate system of the force plate during the data collection phase was also obtained in a different coordinate system than the one used in *OpenSim*. From the registered center location on the force plates, the sensors registered the orientation of the participant as +X anteriorly, +Y towards the left, and +Z vertically down. Whereas *OpenSim* adopts the standard biomechanics coordinate system, where the orientation of the model was +X anteriorly, +Y vertically up, and +Z towards the left. This was accounted for by applying a coordinate transformation to the force plate data, in addition to calculating the free moment and center of pressure on the force plate for each participant.

Both the force plate and marker data were then filtered by applying a 4^{th} order dual-pass Butterworth filter at 15 Hz. In addition, the stop-jump landing time was also calculated for each participant and was defined by the first non-zero data frame for the vertical axis (+Y) after it had undergone calibration, transformation, and filtering. The transformed and filtered data was then reformatted to *OpenSim* compatible file formats, namely the *.trc* and *.mot* file extensions for the marker files and force plate files respectively.

At this point, the full-time frame of the data remained 5 s long. The next section will describe how *OpenSim* was used to crop the trials to a shorter time window of interest and generate a set of muscle forces involved in executing the stop-jump landing.

3.2 *OpenSim*

The *OpenSim* results from this current study have been computed using the 3.2 version of the software. To obtain the final muscle force values, base models were scaled to each participant's anthropomorphic proportions, inverse kinematics were calculated to obtain joint angles, and RRA was computed as a priming step to minimize residual errors. Once these steps were completed, the CMC function was able to solve for dynamic muscle force values throughout the landing trial.

3.2.1 Scaling

Each participant's custom *OpenSim* model was scaled to their respective anatomical proportions from a base developed by Bakker (2014). This model was a modified version of the generic model Gait2392 provided by *OpenSim*. Modifications include doubling the maximum achievable isometric contraction for each of the lower limb muscles due to the generic model being designed for low impact activities such as normal gait. As this study was only interested in the right leg biomechanics, muscle components in the trunk and

left leg were also removed from the Gait2392 model and replaced with torque actuators to reduce simulation time.

It was essential to scale the modified Gait2392 base model to the anatomical proportions of each participant, as this affects the moment arm values when computing muscle forces. A 0.5 s segment at the end of each participant's trial, when the participant has stopped moving, was used as a set of static frames to calibrate the proportions of base model.

3.2.2 Inverse Kinematics

To reduce the simulation time required to compute muscle forces in later steps, the time window of the original 5 s long trial was cropped to a 400 ms window which begins 35 ms before each participant's first landing time. Since this study was primarily interested in the biomechanics resulting from the critical time period between ground contact and peak GRF, only a short simulation time window was required. The Computed Muscle Control function used in subsequent required 30 ms of initializing time (J. Hicks, 2018), and an additional 5 ms of buffer time was added to ensure all landing data was preserved. Most non-contact injuries associated with jump landings occur between the landing and peak GRF instances; therefore, events after the peak GRF were not as significant since the forces on the body declined. The 400 ms offered a generous enough amount of time after the peak GRF. For these reasons, the Inverse Kinematics function in *OpenSim*, the tool was run at 35 ms prelanding for a 400 ms duration. Recall from section 2.4.1 that participants were instructed to perform a stop-jump that consisted of jumping forward onto a force plate, taking off vertically and ending the second landing. Hence it was the first landing that was analyzed, rather than the second landing, as the first landing experienced significant posterior GRFs, which the knee would support and stabilize. The second landing was simply a vertical-jump landing whose biomechanical effects have already been studied by Bakker et al. (2016) and Rao (2020).

3.2.3 Reduce Residuals Algorithm and Computed Muscle Control

As mentioned in the background, the *OpenSim* RRA function served to minimize residual forces used to achieve a balance between GRFs and inertial terms calculated from the acceleration of individual body segments (Delp et al., 2007). This was a crucial step in preparing inputs for the CMC function, as it would minimize errors when computing muscle forces. Slight adjustments were made to the kinematics, trunk center of mass

location, and model mass to equilibrate terms to achieve dynamic consistency. Changes made to the tracking weight would determine how close the adjusted joint angles follow those determined by the original input marker trajectories. Meanwhile, the optimal force setting dictated the maximum residual forces and moments required to supplement force and moment shortages and balance Newton's Second Law. These two adjustment factors had opposing effects on the joint errors and the residual forces. Increasing the tracking weights would reduce the joint angle errors, at the expense of increasing residual values. Increasing the optimal force limit would reduce the residuals but increase the joint errors. The RRA function was iterated automatically through several cycles of adjusting tracking weights, optimal force limits, and model mass until tracking errors and residuals converged. The logical workflow of this optimization process is depicted in Figure 3.2.

In the batch code, the optimization conditions for kinematic deviation were set as a 2° limit for rotations and a 15 mm limit for translations, while the residuals limit magnitude was set to 10% of body weight for both forces and moments. These values were chosen based on the RRA recommendations documentation provided by *OpenSim* (*RRA Best Practices*).

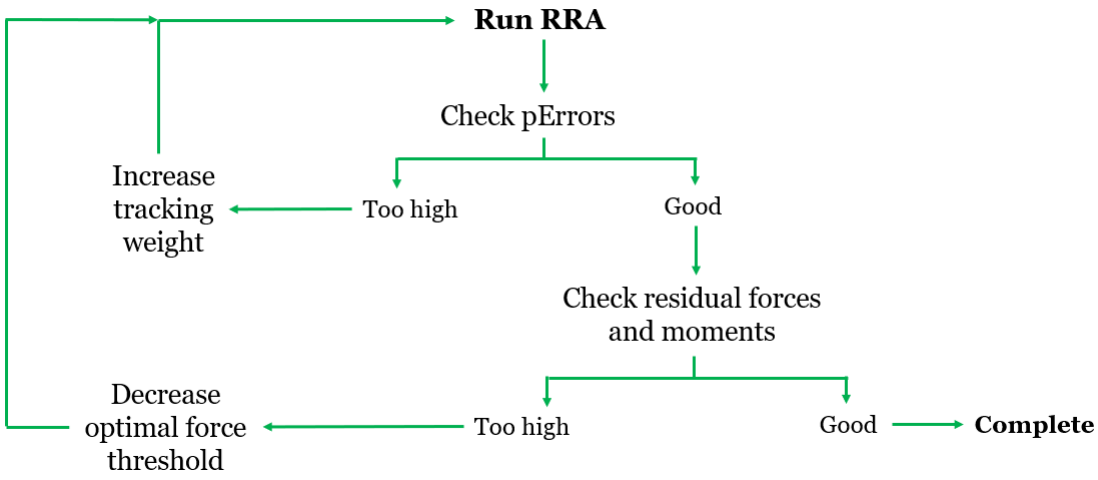

Figure 3.2: RRA batch code workflow

The outcome of this RRA step was a new kinematics and model file with adjusted joint angles, model mass, and torso center of mass location. These parameters played an important role in ensuring that the muscle forces computed in the Computed Muscle Control (CMC) step were solvable while following the original motion as much as possible. The kinematics and kinetics outputs from CMC were used as the final *OpenSim* outputs.

3.3 Muscle Force Processing

The FE model was driven by both kinematics and muscle forces. The kinematics were defined by velocities of the hip and ankle joint in the sagittal plane. The reason why velocities were used as inputs to the simulation rather than displacement values was to follow the high-level process carried out by Rao (2020) for which the FE model was validated for. The idea of using velocities as inputs originates from the nature of the DKS used by Bakker et al. (2016), for which velocities offered a smoother motion output that was less choppy than using displacement curves as inputs. The muscle forces grouping was also based on the DKS design, which had three cables available to represent muscle forces from the quadriceps, hamstring, and gastrocnemius muscle groups. A fourth cable consolidated the remaining thigh muscle forces into a hip moment component. In this study, an improvement was made to the original simulation inputs by including an ankle torque that was previously not accounted for in the DKS. This ankle torque included the effects of the soleus and other plantar flexor muscles connecting the tibia to the foot. Therefore two velocity curves and five muscle kinetics curves were prepared as inputs to the FE simulation. In order to fit the kinematic and muscle force outputs from *OpenSim* to be compatible inputs into the FE knee model, a few processing steps were carried out in a custom *MATLAB* script.

3.3.1 Kinematics

The FE model kinematics were driven by the hip and ankle joint center velocity curves. The hip point was limited to translate along the Y-axis while the ankle was limited to translate along the X-axis. Recall that the reason for this configuration was to mimic the degrees of freedom present in the DKS validated by previous studies (Bakker et al., 2016)(Polak, 2018)(Rao, 2020). Moreover, the velocity inputs also ensured the simulated motion was stable in the absence of frontal plane muscles.

The input velocity of the hip represented the rate of change of the relative vertical distance between the hip and ankle point. Likewise, the velocity of the ankle represented the rate of change of relative anterior-posterior distance between the hip and ankle point. Using the relative distance allowed the ankle and hip to each slide along one axis while preserving the kinematics of the jump landing. The hip velocity acted along the Y-axis while the ankle velocity acted along the X-axis. Therefore the first step of processing the *OpenSim* output kinematics was to obtain the spatial difference between the XYZ position coordinates of the hip from the ankle joint center. Because the motion simulated was

isolated to the sagittal plane, a rotational transformation about the Y-axis was applied to "compress" any rotational motion of the hip and pelvis (Manal & Buchanan, 2004). The equation below shows the transformation matrix used to obtain the sagittal hip flexion angle. The angle θ used to apply the Y-rotational transformation shown below was the sum of the pelvis rotation and the hip rotation angles obtained from *OpenSim* outputs. The transformed displacements were then differentiated to obtain velocity curves for the hip and ankle joint centers.

$$R_y = \begin{pmatrix} \cos\theta & 0 & \sin\theta \\ 0 & 1 & 0 \\ -\sin\theta & 0 & \cos\theta \end{pmatrix}$$

3.3.2 Muscle Forces and Moments

Before grouping muscle force outputs from *OpenSim* into the five kinetic FE model inputs, the forces and moments were first scaled to the anatomical properties of the cadaver knee from which the FE model was constructed from. This was done by calculating the moment contribution of each muscle by multiplying the respective muscle force and moment arm values of each of the five trial participants. It is worthy to note that these individual moment arms were not constant throughout the trial, albeit without varying dramatically. Many muscles can span more than one joint (ie. both knee and hip), and may not have a straight path over curved surfaces (Sherman, Seth, & Delp, 2013). Once the moment contribution of the relevant quadriceps, hamstrings, and gastrocnemius muscles were obtained, it was divided by the moment arms of the *FE knee* so that each trial participant's muscle force values were anatomically scaled to the knee used in the simulations. Once scaled, the relevant muscle components for each group were summed to obtain one curve each for the quadriceps, hamstrings, and calf muscles.

OpenSim also outputted a net hip moment, which was applied at the hip node of the FE model. However, the quadriceps and hamstrings actuations already present on the FE model would indirectly contribute to the net hip moment. Therefore an adjusted hip moment was applied to the FE model, where the hip moment contributions of the hamstrings and quadriceps muscles were subtracted to prevent double-counting. The ankle moment was applied in a similar fashion on the ankle node of the FE model. The calf muscle input already contains muscle force contributions from the medial and lateral gastrocnemius; therefore, these components were subtracted from the net ankle moment output by *OpenSim*. The adjusted ankle moment represented contributions from the soleus and foot plantar flexor muscles, including the tibialis, peronious, digitorum, and hallucis muscles.

3.4 Finite Element Analysis in *Abaqus*

3.4.1 Initializing Knee Flexion

As described in the Background chapter, a stop-jump differs from a vertical-jump landing in that the person is jumping forward rather than falling from a vertical drop. Therefore the stop-jump landing participants had their knees flexed at the start of the trial unlike vertical-jump landings where the leg was relatively straight. Different participants had different initial flexion angles, as shown in Table 3.2. Therefore for each simulation, the knee model was flexed to the correct starting flexion angle for the forces and kinematics to be applied at the correct orientation, as depicted in Figure 3.3. The flexion angle of the FE model in its original state was about 12°, as this was the resting angle of the cadaver knee during the process of creating the FE model from MRI and CT scans (Rao, 2020). If the knee was not flexed to the correct start flexion angle, the vectors would be applied at incorrect orientations and directions, leading the simulation to abort due to unrealistic movement.

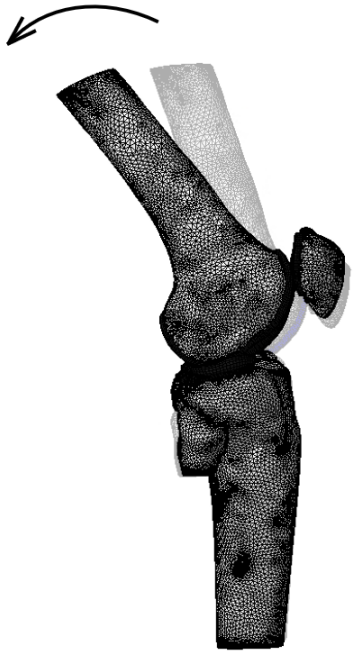

Figure 3.3: FE flexion step

Table 3.2: Initial flexion angles at the start of the trial.

	P1	P2	P3	P4	P5
OpenSim Initial Knee Flexion (°)	24.63	33.96	13.80	26.13	23.50
FE model Initial Knee Flexion (°)	25.74	36.24	13.63	26.85	24.00

In addition to setting the orientation correctly, coordinate transformations were applied to ensure that these displacements were in the FE knee model's local coordinate system. The coordinate system followed that of *OpenSim* where anterior was +X, superior was +Y, and right was +Z. The origin was located at the intersection of a vertical axis drawn from the hip down and a horizontal axis drawn from the ankle node. A depiction of the coordinate system can be referenced in Figure 2.12.

The knee center node used in *OpenSim* was located inside the bone and was not visible in the GUI. Therefore less estimation would be involved by using an *OpenSim* reference on the surface of the bone where one could also visually locate the equivalent position on the FE model. Therefore a coordinate very close to the actual *OpenSim* knee center (0,0,0) was used for reference, which was the (0,-0.01,0) coordinate, 1 cm below the actual knee center. This node was used to ensure that the limb lengths of the FE model matches each of the participants. It was understood that this was not the knee joint center node, and also would not affect that accuracy of flexion angle measurements from the simulation results because the femur condyle did not deform throughout the trials.

In *Abaqus CAE*, a step was created to achieve the correct initial flexion angle. The femur was flexed in the first half of the step, where the hip node was displaced downwards and posteriorly to its relative X and Y distance from the knee center node. During this step, the ankle was fixed. This was followed by the second half of the step, where the ankle node was displaced upwards and anteriorly, while the hip node was fixed in its new position. This flexion step not only ensured that the knee begins at the correct flexion angle but was also rotated at the correct orientation with respect to the X and Y-axis.

3.4.2 Kinematic Boundary Conditions

The simulation boundary conditions are shown below in Figure 3.4. The hip node was constrained to translating only along the vertical Y-axis while being fixed in the X and Z-axis. Its rotation about the X and Y-axis was also fixed while being free to rotate about the Z-axis. The ankle was unconstrained in all degrees of freedom except for controlled

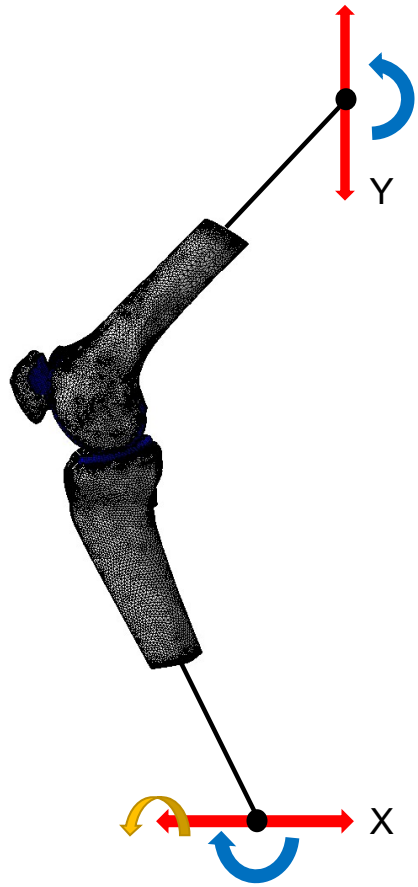

Figure 3.4: Kinematic boundary conditions

translation along the X-axis and being fixed in the Y-axis. Recall that many of the boundary conditions used in the FE simulations of this study were adapted from the *in-vitro* jump landing studies conducted on the University of Waterloo DKS. The behavior of the hip kinematics for this simulation originated from the nature of the DKS hip node being mounted on a vertical track while the ankle node was designed with a horizontal track mounted with joints that allowed for motion in all degrees of freedom except for being anchored to the horizontal track. This combination of kinematic boundary conditions allowed the jump-landing motion to be replicated in *Abaqus*. With these boundary conditions, the velocity input curves were applied to reference points at the extremities of the femur and tibia which represented the hip and ankle joint center locations.

3.4.3 Joint Moment Boundary Conditions

The two joint moment inputs were applied to the same hip and ankle reference points used for the kinematic inputs. Since the motion was isolated to the sagittal plane, both the ankle and hip moment acted exclusively about the Z-axis.

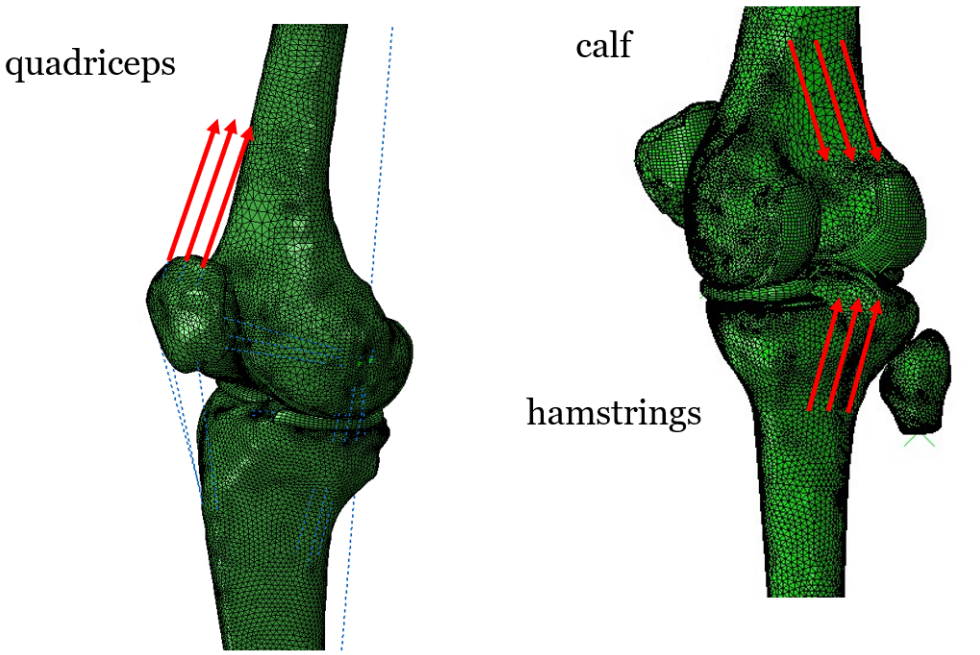

Figure 3.5: Quadriceps, Hamstrings, and Calf FE forces (only three quadriceps vectors shown for simplified visualization).

The remaining three muscle inputs were applied at node locations on the knee model, which reflected the muscle attachment sites of the original cadaver specimen from which the landmarks were digitized. Their application points were defined by vectors that pointed towards their respective muscle fibre trajectories, as shown in Figure 4.6. The hamstrings and gastrocnemius forces were both uniformly distributed among three vectors each, with the hamstring acting on the tibia and the gastrocnemius muscles acting on the femur. The quadriceps muscle force was significantly greater than the gastrocnemius and hamstring forces for all participants and was therefore distributed uniformly among seven vectors, applied at the patella.

3.4.4 Anatomical Properties and Strain Measurement

The quadriceps forces computed for P2, which is presented in the next chapter under Results, were particularly high compared to the other participants. This generated excessive element distortions in the patellar and femoral cartilage regions. To mitigate this effect, the patellar tendon stiffness was increased by a factor of 2 from its original of 180 N/m to 360 N/m. This was done for the P2 simulation only. Increasing the patellar tendon stiffness helped stabilize the patella by opposing the high quadriceps forces for this particular participant. To ensure that this adjustment did not have an effect on the ACL strain, a test simulation was performed on a different participant to compare the ACL strains from the anatomical stiffness condition to the doubled stiffness condition. The P1 simulation completed successfully without excessive distortions using the anatomical patellar tendon stiffness and it was simulated again for these reasons at the increased stiffness value.

ACL and Meniscal Strain

The ACL strain ϵ was defined by the engineering strain formula, where it was a function of the change in length over the original gauge length:

$$\epsilon = \frac{\Delta L}{L_0}$$

In the FE knee model, the length of the ACL in its original state was 315 mm, defined by the distance between its connector attachment nodes shown in Figure 3.6. However, as a result of the flexion step at the start of the simulation, the length of the ACL changed. Therefore the gauge length L_0 was set as the ACL length at the end of the flexion step. Following the flexion step, there was a 100 ms ramp-up time where the muscle forces and moments were increased linearly from zero. The rationale for this was to avoid excessive element distortions as well as large spikes in the simulation's kinematic energy. During the ramp-up period, as the muscle forces and moments began to exert their effects on the knee ligaments, the ACL length changed notably. Therefore to account for these changes, the ACL gauge length was defined as the length at the start of the ramp-up period, in its already flexed state. If the gauge length was taken at the end of the ramp-up period, in other words at the start of the *OpenSim* trial, the strain calculated would not fully account for the ACL length displacement ΔL resulting from the application of the muscle forces and moments. Hence each participant's strain is calculated with a slightly different gauge length.

To compute the meniscal strain, the gauge length was also taken at the beginning of the ramp-up period for the same reasons. The meniscal strain gauge length was defined as the distance between two nodes located on the posterior medial meniscus, as shown in Figure 3.7.

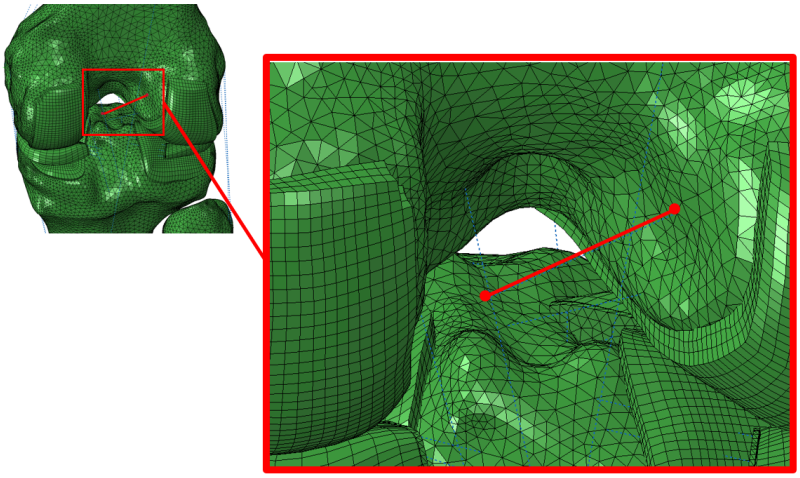

Figure 3.6: ACL attachment in the FE knee model

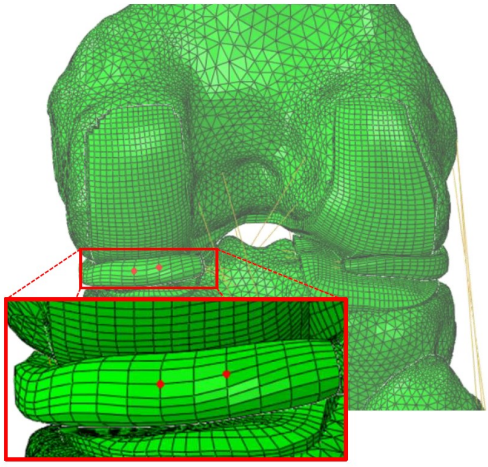

Figure 3.7: Meniscus reference points in the FE knee model. Image adapted from Rao (2020).

3.4.5 Simulation Timeline

The entire FE simulation spanned 770 ms in *Abaqus* and is depicted in Figure 3.8. The first 400 ms was where the flexion step occurred. The next 100 ms of the simulation served to pre-load the model by linearly ramping up the muscle forces and moments from zero. The remaining 270 ms of simulation time was where the jump-landing took place and breaks down to 5 ms of prelanding time, followed by 265 ms of landing impact time. This 270 ms jump landing window includes the peak GRF instance for all five participants. Every simulation was conducted on a 64-bit, 32.0 GB RAM, Intel® CoreTM i7-5960X CPU.

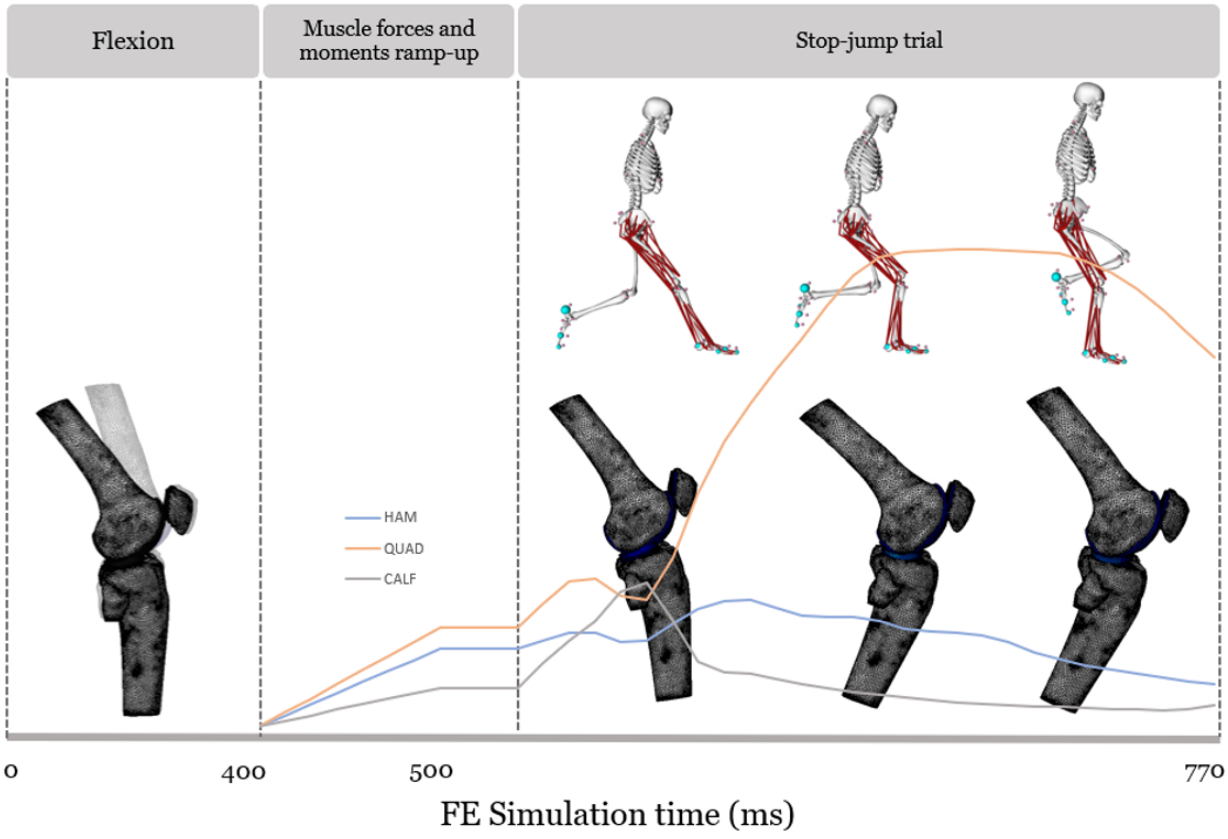

Figure 3.8: FE simulation timeline

3.5 Statistical Analysis

To understand the relationship between notable biomechanical parameters and their effects on ACL and meniscal strain, bivariate and multivariate analysis was conducted on the results.

3.5.1 Bivariate Analysis

26 kinematic and dynamic parameters were compared to both ACL and meniscal strain. The following parameters shown in Table 3.3 were obtained from the *OpenSim* outputs and were compared at both the maximum value for the entire trial and also the corresponding value at the instance of maximum GRF.

Table 3.3: Statistical analysis parameters, with kinematic and dynamic parameters extracted at trial peak and at maximum GRF instances.

Body mass	-
GRF	-
Sagittal flexion/extension angles	Ankle, Knee, Hip, Trunk
Sagittal moments	Ankle, Knee, Hip, Trunk
Muscle Forces	Quadriceps, Hamstrings, Gastrocnemius
Range of flexion	Knee, Hip, Knee/Hip
Angular Velocities	Knee, Hip

Pearson correlation values were computed comparing each parameter to the participants' resulting ACL and meniscal strains. These Pearson coefficient values were then tested for statistical significance using permutation testing. The advantage of using permutation testing rather than employing the T-test was that it was well-suited for small sample sizes, as it does not assume the data follows a normal distribution. Instead, the response was permuted to generate $n!$ randomized Pearson correlation values, where n was the number of data points, in this case five. The p-value was then obtained by calculating what proportion of randomized Pearson values were as extreme as the one observed. If the p-value was less than the significance threshold, the Pearson correlation was considered statistically significant (Howell, 2015).

3.5.2 Multivariate Linear Regression Modeling

In certain cases, individual parameters may not be linearly correlated with the response on their own. However, when paired with one or more parameters, a strong linear regression model can be observed. Hence a multivariate linear regression analysis was also conducted on the data to observe whether there was a statistically significant relationship between the strains compared to two or more variables. Statistical computations were performed using RStudio 1.4.1717. A linear regression model could have as many as $n - 2$ variables, therefore the linear regression equations presented in this study could potentially contain one to three variables. An iterative process of educated trial-and-error combined with the "model reduction" approach was used to identify a linear model that was statistically significant. The "model reduction" approach was applied by judging the p-value of each coefficient and replacing a variable with a high p-value with one that yields a lower p-value (Minitab, 2019). The p-values determined from the bivariate analysis also served as potential indicators for providing an educated guess as to which variables would yield a statistically meaningful model. The model with the highest adjusted R-squared value and lowest p-values were then taken as the best regression equation.

Chapter 4

Results

There were three main phases of results obtained for this study. The first phase consists of the *OpenSim* outputs which include the main lower limb muscle forces, joint moments for the hip and ankle, as well as the kinematics of the stop-jump landing. These *OpenSim* results were the inputs for the FE simulations in *Abaqus*, which generates the ACL and meniscal strain curves. Finally, the relevant sagittal plane parameters were compared to the peak strain values to conduct a statistical analysis of their correlations and relationships in the form of multivariate linear regression models. All of the plots shown in this chapter represent the results beginning *after* the flexion step and is set to zero starting from this point onward, equaling 370 ms of results out of the total 770 ms of simulation time.

4.1 *OpenSim* Results

Detailed properties of each study participant were presented in Table 3.1 from the Methods chapter. The average body mass of the five participants (three female, two male) was about 68 kg, with varying jump speeds that average to about 194 ms from the instance of toe contact with the ground to peak GRF.

4.1.1 Kinematics and Muscle Forces

Both the velocities and displacements for the hip and ankle node are shown in Figures 4.1 and 4.2 respectively below. Note that the hip and ankle curves represent two different axes, with the hip being constrained to the Y-axis while the ankle was constrained to the

X-axis. The velocity trajectories were used as the inputs to the FE simulation and were differentiated from the displacement outputs obtained from *OpenSim*. The first vertical dotted line represents the beginning of the trial since the first 100 ms of the simulation represents the forces and moments ramp-up period. The second vertical dotted line marks the instance of landing where the foot has made contact with the ground.

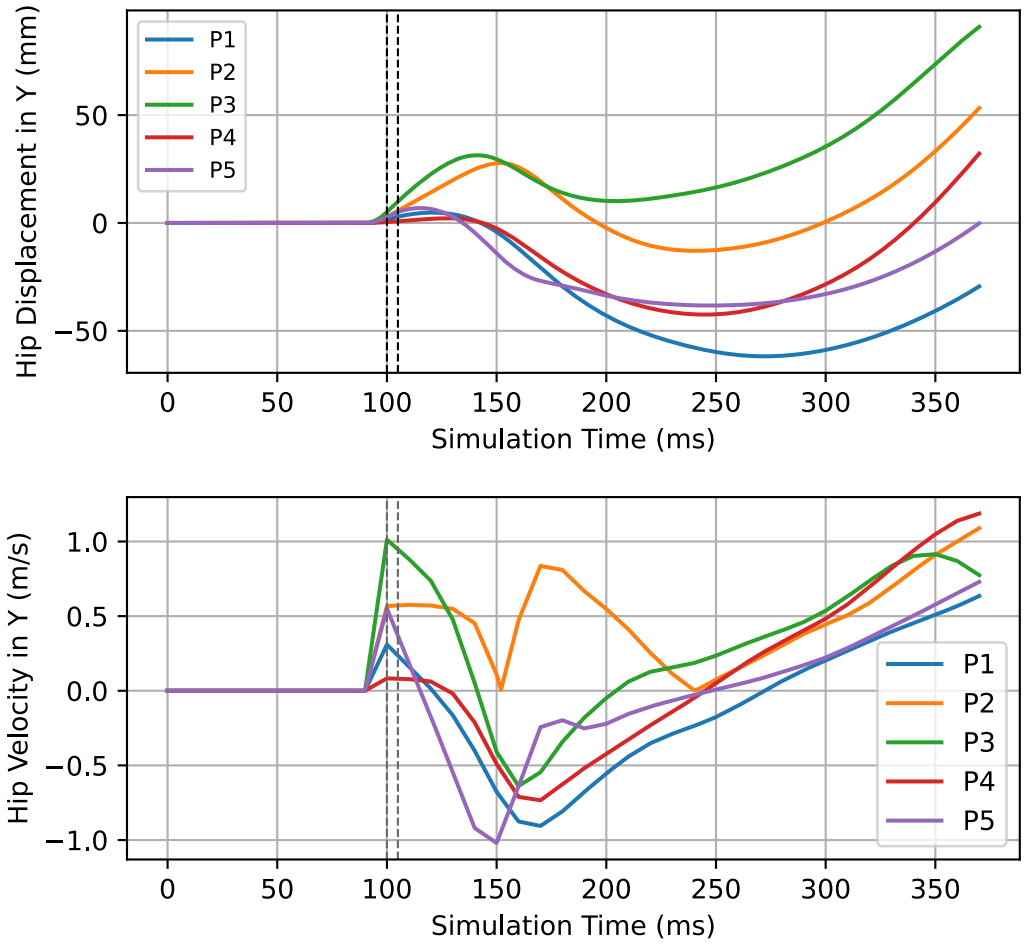

Figure 4.1: Hip displacement and velocity along the Y-axis. The first dashed line represents the end of the muscle force ramp-up period and the start of the jump trial. The second dashed line represents the instance of landing, defined by the beginning of ground contact.

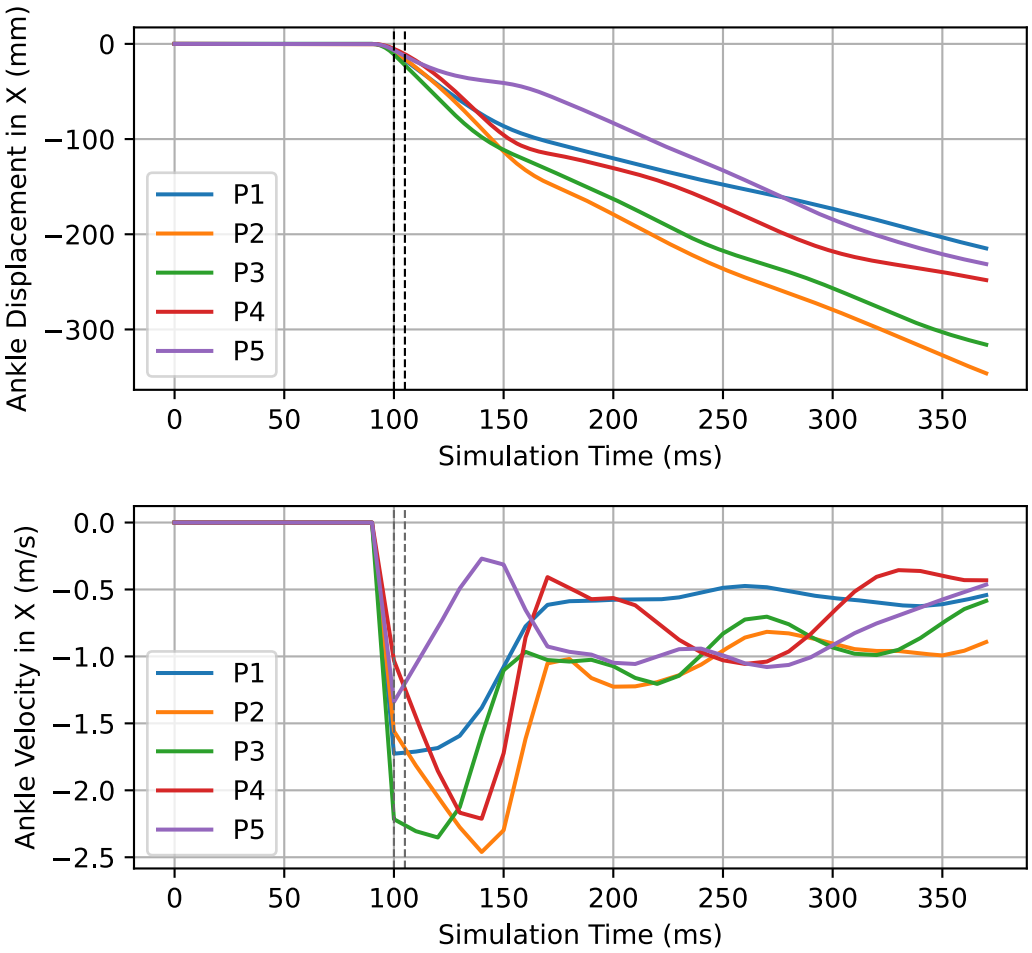

Figure 4.2: Ankle displacement and velocity along the X-axis

Muscle forces which were grouped according to the method described in Section 3.3.2 are presented in Figure 4.3.

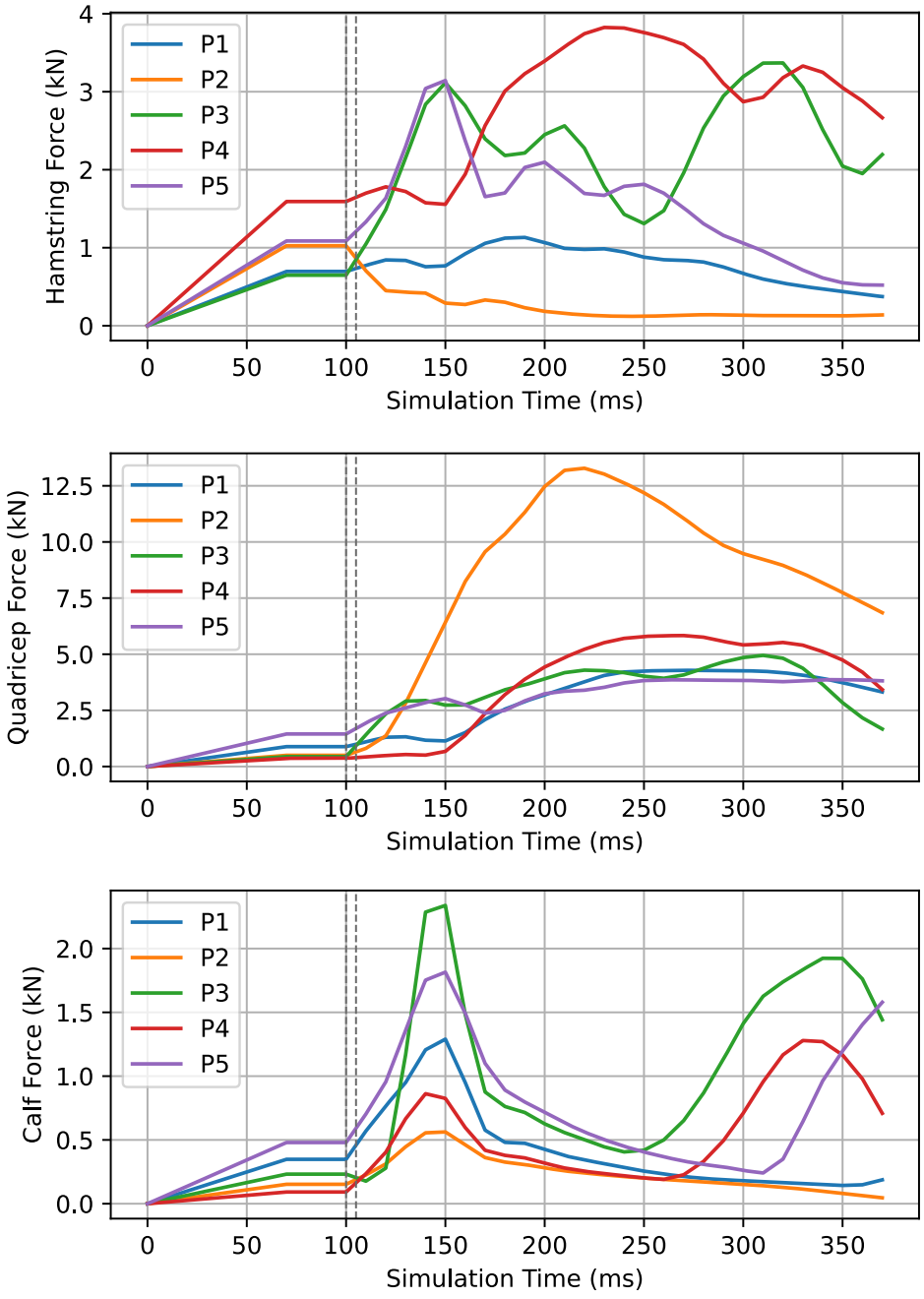

Figure 4.3: Forces for hamstring, quadriceps, and calf muscles

Table 4.1 summarizes the residual and positional errors from the Opensim results. All residual forces and moments were found to be roughly 5% or less of the peak external value. The maximum external force refers to the peak GRF for each participant, while the maximum external moment was a function of the peak GRF multiplied by the vertical component of the participant's center of mass location. The positional errors (pErrors) refers to the linear or rotational deviation of marker points from their prescribed kinematic trajectories.

Table 4.1: Peak residuals and pErrors of *OpenSim* muscle force results

	P1	P2	P3	P4	P5
Residual Force (%Max External Force)	5.18	1.62	1.19	0.79	0.67
Residual Moment (%Max External Moment)	3.53	4.53	2.94	2.76	3.91
Translational pError (mm)	8.49	28.80	14.01	30.61	17.78
Rotational pError (°)	0.10	0.13	0.06	0.05	0.05

* Values shown are absolute and do not specify direction.

4.1.2 Joint Moment FE Simulation Inputs

The positive values of the internal joint moment curves shown in Figure 4.4 represent extension moments, while negative values represent flexion moments for the hip and ankle curves. These hip moment results represent the values used as inputs into the FE simulation, and have had the quadriceps and hamstring contributions subtracted. Likewise, with the ankle moment shown in Figure 4.4, they have had the gastrocnemius muscle contributions subtracted.

It was noted that P2 behaves as an outlier to the other four participants for both the hip and ankle, where the hip moment acts in flexion instead of extension, and likewise for the ankle.

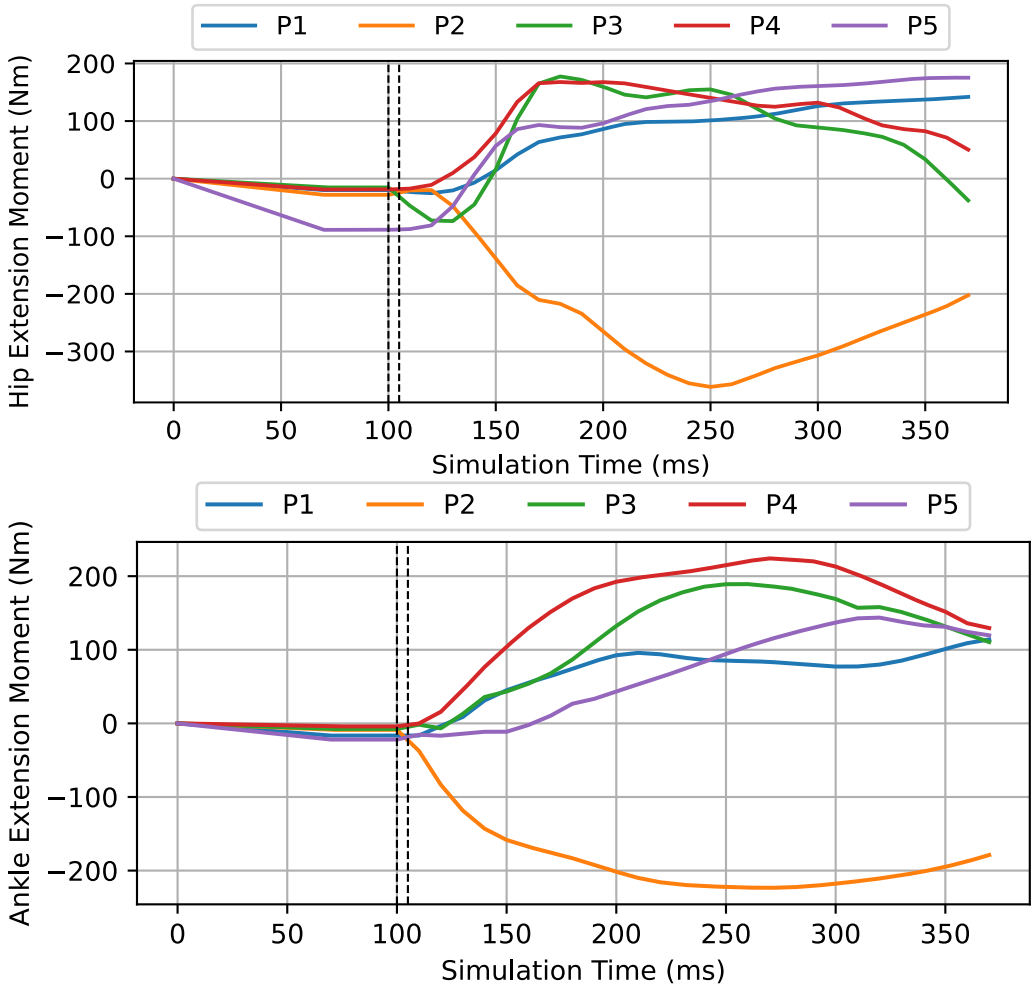

Figure 4.4: Internal hip and ankle moments in the sagittal plane

4.2 Finite Element Simulation Results

ACL and meniscus strains are plotted below in Figure 4.5, beginning from the force ramp-up period, which immediately follows the knee flexion step. The reasoning behind this was to capture the changes in ACL and meniscus deformation as soon as the forces and moment begin gradually activating.

4.2.1 Strain Results

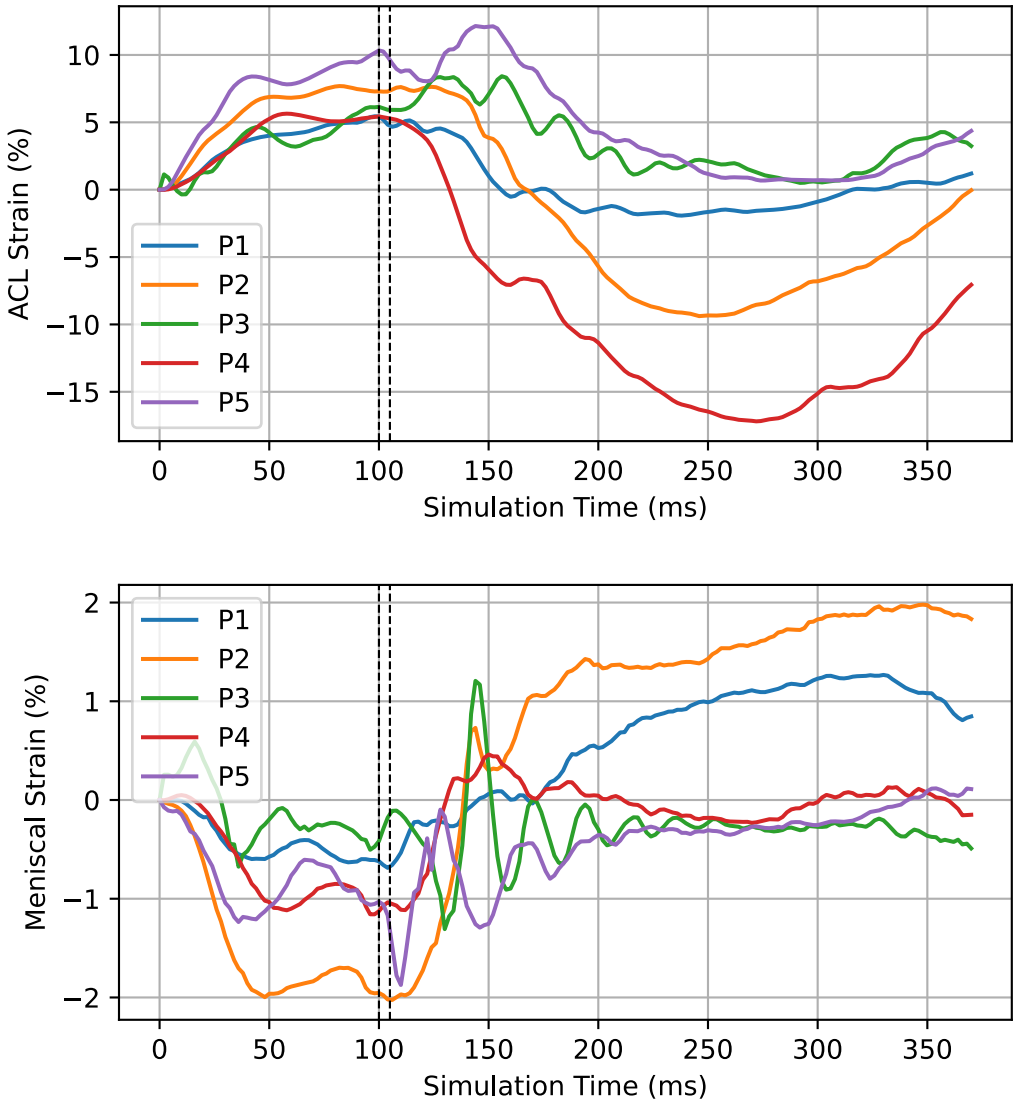

Figure 4.5: Strain values with the gauge length beginning at the end of the flexion step

Table 4.2: Peak strain values

	P1	P2	P3	P4	P5	Mean
ACL Gauge Length (mm)	31.66	31.52	29.85	31.69	31.24	31.19
Meniscus Gauge Length (mm)	12.73	12.79	12.70	12.73	12.78	12.75
Peak ACL Strain (%)	5.44	7.69	8.42	5.64	12.15	7.87
Time to Peak ACL Strain (ms)	98	82	156	58	144	108
Peak Meniscal Strain (%)	1.27	1.98	1.21	0.46	0.12	1.01
Time to Peak Meniscal Strain (ms)	330	348	144	150	354	265

* Time values begin counting after the flexion step, at the start of the force and moments ramp-up period.

4.2.2 Knee Kinematic Results

Figure 4.6 shows knee flexion from *OpenSim* outputs and *Abaqus* outputs being compared to ensure that the knee flexion angle throughout the jump landing was representative of the marker data, since the motion was driven only at the ankle and hip node.

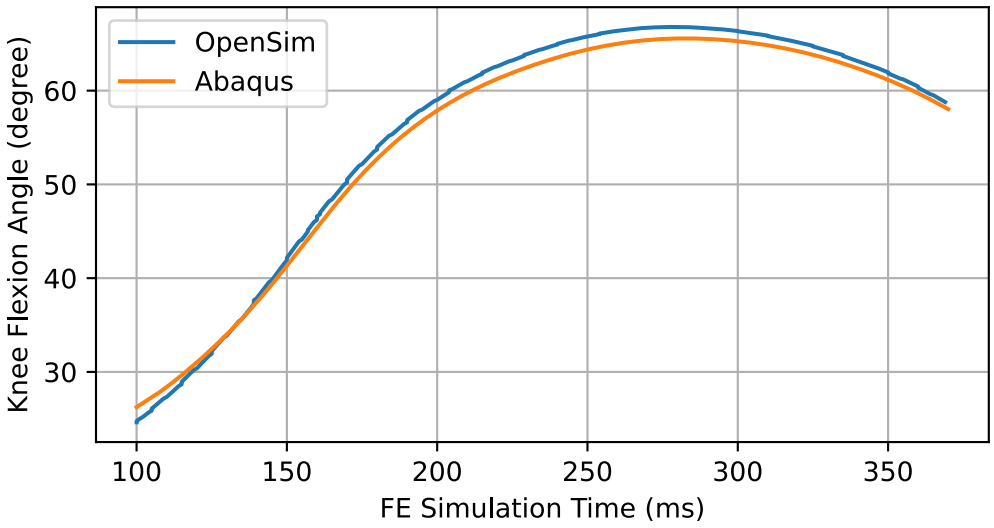

Figure 4.6: Knee flexion angle comparison between *OpenSim* and *Abaqus* outputs for P1. The plot starts at 100 ms, which marks the start of the jump trial.

4.3 Statistical Analysis

A compilation of the major sagittal plane parameters was summarized for each participant in Table 4.3 for the maximum values of the whole trial and the peak GRF value. The variables at peak GRF offered an equivalent condition for comparison while it was not necessarily the maximum over the entire trial. Note that the *total* joint moments reported in Table 4.3 included the contributions from all active muscles. This should not be confused with the *net* joint moments used as inputs at the hip and ankle node presented in Figure 4.4.

Table 4.3: Summary of sagittal plane parameters

Data	**Condition**	**Parameters**	**P1**	**P2**	**P3**	**P4**	**P5**
Kinematics Angles (°)	Max. of trial	Ankle flexion	25.79	29.87	6.66	17.72	20.48
		Knee flexion	66.79	69.50	50.55	63.74	57.47
		Hip flexion	55.49	53.61	53.51	71.12	62.02
		Trunk flexion	8.23	23.31	7.28	12.52	7.99
	At Max. GRF	Ankle flexion	25.74	29.87	6.33	17.16	20.31
		Knee flexion	65.10	68.00	50.54	63.65	56.70
		Hip flexion	51.39	44.76	50.82	70.34	52.94
		Trunk flexion	4.33	22.61	7.18	11.89	7.33
Joint Moments (Nm)	Max. of trial	Knee extension	140.14	669.61	130.49	94.62	96.56
		Hip extension	127.17	30.57	236.92	332.75	186.91
		Trunk extension	101.29	18.53	222.15	277.91	174.12
	At Max. GRF	Knee extension	138.54	669.13	130.30	82.89	95.53
		Hip extension	117.21	-359.85	158.48	309.21	143.57
		Trunk extension	101.05	-336.54	126.81	263.29	128.39
Muscle Forces (N)	Max. of trial	Quadriceps	4284.78	13282.50	4948.71	5832.43	3868.44
		Hamstrings	1131.81	1025.07	3369.17	3824.25	3143.56
		Gastrocnemius	1289.93	562.51	2338.11	1279.02	1815.02
	At Max. GRF	Quadriceps	4168.60	9452.89	4132.30	5785.45	3780.65
		Hamstrings	541.63	133.65	1392.57	3765.52	847.39
		Gastrocnemius	164.64	150.76	409.84	203.30	338.45
Range of Flexion (°)	At Max. GRF	Knee	40.47	34.04	36.73	37.52	33.20
		Hip	16.21	-8.85	6.31	15.73	3.19
		Knee/Hip	2.50	-3.85	5.82	2.38	10.42
Angular Joint Velocity (°/s)	At Max. GRF	Knee	79.61	71.70	-8.08	-23.60	64.15
		Hip	174.97	112.81	46.37	79.89	166.11
		Knee/Hip	0.45	0.64	0.17	0.30	0.39

* Negative values represent the direction opposite to the parameter label.

Pearson correlation coefficients with ACL and meniscus strain are both tabulated in

Table 4.4 below to provide a broad summary of which sagittal plane parameters can be the best candidates for strain behavior predictors. The p-value is also presented, where values lesser than 0.1 were considered statistically significant.

Table 4.4: Pearson correlations between maximum ACL and meniscus strain and sagittal plane parameters

Data	**Condition**	**Parameters**	**Max ACL Strain**		**Max Meniscal Strain**	
			Pearson Coefficient	**P-Value**	**Pearson Coefficient**	**P-Value**
Kinematics Angles	Max. of trial	Ankle flexion	-0.167	0.775	0.357	0.533
		Knee flexion	-0.513	0.425	0.418	0.500
		Hip flexion	-0.093	0.825	-0.750	0.183
		Trunk flexion	-0.189	0.733	0.628	0.267
	At max. GRF	Ankle flexion	-0.159	0.792	0.365	0.533
		Knee flexion	-0.537	0.367	0.393	0.517
		Hip flexion	-0.332	0.508	-0.649	0.217
		Trunk flexion	-0.073	0.917	0.549	0.333
Joint Moments	Max. of trial	Knee extension	-0.069	0.825	0.792	0.025*
		Hip extension	-0.101	0.858	-0.713	0.167
		Trunk extension	0.000	1.000	-0.730	0.150
	At max. GRF	Knee extension	-0.059	0.833	0.796	0.025*
		Hip extension	-0.075	0.942	-0.786	0.125
		Trunk extension	-0.061	0.983	-0.796	0.108
Muscle Forces	Max. of trial	Quadriceps	-0.153	0.717	0.738	0.150
		Hamstrings	0.270	0.742	-0.753	0.208
		Gastrocnemius	0.413	0.517	-0.493	0.400
	At max. GRF	Quadriceps	-0.243	0.608	0.665	0.208
		Hamstrings	-0.342	0.508	-0.538	0.392
		Gastrocnemius	0.639	0.242	-0.417	0.450
Range of Flexion	At max. GRF	Knee	-0.806	0.075*	0.125	0.842
		Hip	-0.496	0.367	-0.481	0.450
		Knee/Hip	0.65	0.216	-0.512	0.375
Angular Joint Velocity	At max. GRF	Knee	0.221	0.808	0.314	0.558
		Hip	0.190	0.767	-0.164	0.758
		Knee/Hip	-0.067	0.900	0.528	0.358

* The p-values of Pearson correlations which were statistically significant are labeled with a '*'.

Many different regression models were tested for both the ACL and mensicus strain relationships using a permutation testing approach to determine statistical significance. The models with the strongest statistical significance and best R^2 values are presented

below. The best regression model for ACL strain includes two parameters while the best model for meniscus strain includes one parameter, where ROF is the range of flexion.

Table 4.5: Peak ACL strain regression model

Variable	Coefficient	P-Value
Constant	7.87	-
Knee ROF (Peak GRF)	-0.94	0.025
Quadriceps Force	-0.001	0.10
Adjusted R^2: 0.91	Model P-Value: 0.044	

Peak ACL Strain = 7.87 - 0.94(Knee ROF at Peak GRF)
- 0.001(Quadriceps Force)

Table 4.6: Peak meniscal strain regression model

Variable	Coefficient	P-Value
Constant	1.006	-
Knee Ext. Moment (Peak GRF)	0.0023	0.025
Adjusted R^2: 0.51	Model P-Value: 0.10	

Peak Meniscal Strain = 1.006 - 0.0023(Knee Ext. Moment at Peak GRF)

Chapter 5

Discussion

Applying a FE modeling approach to study the biomechanical responses of the knee joint during stop-jump tasks has opened up a new field of possibilities for quantitative findings that can significantly contribute to injury prevention and rehabilitation techniques. At the time of this project, this was the first study that used a combination of numerical and FE modeling tools to closely analyze the strain behavior of the ACL and meniscus during a single-leg stop-jump maneuver. The ability to calculate real-time muscle forces from *OpenSim* was coupled with the increased accuracy of simulating these outputs on a more anatomical representative computational knee model in *Abaqus*. This approach allowed movements to be replicated and replayed with a frame-by-frame insight of how the kinematics, muscle forces, and joint moments collectively influence the knee joint.

The purpose of this study was to use *OpenSim* and FE modeling to investigate how various kinematic and kinetic sagittal plane parameters contribute to ACL and meniscus strain during a single-leg stop-jump task. Validation measures were taken at every major step executed in this study to ensure that the intermediate outcomes were obtained correctly and that the simulation results were anatomically representative of *in-vivo* biomechanical behavior. In addition to analyzing the kinematic patterns and muscle force values compiled by *OpenSim*, residual and pError values were also measured to ensure that, before inputting values into the FE model, the raw inputs data was largely unchanged throughout the Scaling, Inverse Kinematics, RRA and CMC steps. Likewise, joint kinematics were verified for the FE simulation outputs to confirm that the dynamics of the original motion was preserved. Finally, peak strain values from the ACL and meniscus were compared against the main kinematic and kinetic sagittal plane parameters in a bivariate and multivariate regression analysis to support observations on strain behavior throughout the simulation

time. A randomization approach using permutation testing was well-tailored to this study as it allows for statistically meaningful conclusions to be drawn from a smaller sample size.

5.1 Kinematic Contributions

5.1.1 Validation of Kinematics

To first establish that the resulting kinematics simulated by the FE model were reflective of the original marker data trajectories, the positional errors listed in Table 4.1 as well as the comparison plot in Figure 4.6 indicated that there was very little deviation. Both the peak translational and rotational pError adjustments resulting from the all of the *OpenSim* computations fall well under the 5 cm and 5° limit of what was considered acceptable by the *OpenSim* best practices documentation (*RRA Best Practices*). Furthermore, while velocities were used as inputs rather than directly applying displacement values into the FE model, the positional outputs of the simulation were still equivalent to the *OpenSim* results as shown in Figure 4.6. The congruency of the knee flexion curves show that there was little difference in knee flexion angle between the simulation outputs in *Abaqus* compared to outputs from *OpenSim*.

5.1.2 Flexion Angle and Strain Behavior

The kinematics of a jump maneuver can play a significant role in the resulting risk of ACL and meniscus injury (Roy et al., 2015; Leppänen et al., 2017). Greater likelihood of ACL damage has been linked to "stiff" landings, where there was a low knee and hip flexion (Leppänen et al., 2017). This finding was further confirmed by several other studies carried out on vertical-jump landings (Bakker et al., 2016; Blackburn & Padua, 2008). A study by Decker et al. (2003) also explains that increasing knee flexion during the ground contact phase of drop landings stretches out the time taken to reach peak knee extension moments and increases the shock absorbency in the knee joint, particularly in young female athletes. However the relationship between reduced flexion angles and increased strain may differ in stop-jump landings compared to vertical-jump landings, as there was a much greater posterior GRF arising from the forward momentum of a stop-jump. As a different muscular strategy was used to counter these different ramp-ups, the relationship between joint flexion angles and strain in a stop-jump may be more complex.

Knee Flexion

The knee flexion angles observed in this study have been found to fall within the typical range of values observed in other stop-jump studies. The three studies shown below in Table 5.1 performed two-leg stop-jump landing tasks, all from healthy physically active young participants. The values from Dai et al. (2019) were obtained from jumps executed at 60% of maximum achievable height while Kar and Quesada (2012) asked an all-female group to jump onto a forceplate from a 50 cm high platform. Participants from Yu et al. (2006) took a running approach before landing with both feet on the forceplate. The knee flexion values obtained from this current study fall well within the common range of flexion angles for stop-jump tasks, indicating that none of the participants performed the maneuver irregularly in terms of knee joint motion.

Table 5.1: Mean peak knee flexion angles

	Gender	Mean Knee Flexion (°)	SD
Current study	Male and Female	61	±6.3
Dai et al. (2019)	Male and Female	67	±7.6
Kar & Quesada (2012)	All Female	57	±5.3
Yu et al. (2006)	Female	69	±9.3
Yu et al. (2006)	Male	77	±10.6

In this study, there was a moderate correlation between increased ACL strain and lower knee flexion angles, particularly at the peak GRF time, with a Pearson Coefficient of -0.51 as seen in Table 4.4. In fields such as medicine, an absolute Pearson Coefficient greater than 0.5 is generally considered to show a moderate correlation (Mukaka, 2012). It was noted that the p-value was high for statistical significance, however given the small sample size of participants in this study with an already moderate correlation between these parameters, the likelihood of a stronger underlying correlation should be considered. Looking closer at Table 4.3 shows that if one excludes P2, a high Spearman's coefficient of -0.8 (p=0.2) can be calculated for the ranking correlation between ACL strain and knee flexion at peak GRF. This observation agrees with the trend that high knee flexions were strongly associated with reduced ACL strain and can be recommended for injury-preventing landing practices in stop-jump activities.

Knee Range of Flexion

The level of statistical significance adopted for this study was 0.1. The most common values for statistical significance are 0.01, 0.05, and 0.1 (Filho et al., 2013), where the stringency depends on the field of study. It is most common to see studies use 0.05 as a significance threshold (Dahiru, 2008), however this value was established arbitrarily in the 1920s, and certain applications such as clinical trials for pharmaceuticals may require a much more strict significance level (Kim & Choi, 2019). An α value of 0.1 was deemed significant for this study as it was adjusted to a small sample size and describes a biomechanical behavior where slight differences in position, force or moment will not significantly change ACL nor meniscus strain values.

Having established the statistical significance threshold, one can observe that the knee range of flexion has a strong negative correlation with ACL strain. The knee range of flexion was defined as the net angular difference between the knee flexion at the time of landing and the time of peak GRF. Participants exhibited on average an additional flexion of 36° from the time of foot contact to each of their respective maximum GRF times. A greater range of knee flexion post-landing was found to be highly correlated with reducing ACL strain, with a statistically significant Pearson coefficient of -0.8. This observation, combined with the moderate correlation found between high knee flexion angle and reduced ACL strain suggests that knee flexion at a single frame alone may not be enough to alleviate force on the ACL. The difference between the two parameters is that one can land in a very flexed knee position at peak impact force and still experience a high risk of ACL injury if they maintain a relatively rigid knee angle that does not increase sufficiently over time. This subtle distinction better characterizes a "soft" landing and is especially significant in stop-jump tasks where the knee begins at an already much more flexed position compared to a vertical drop landing.

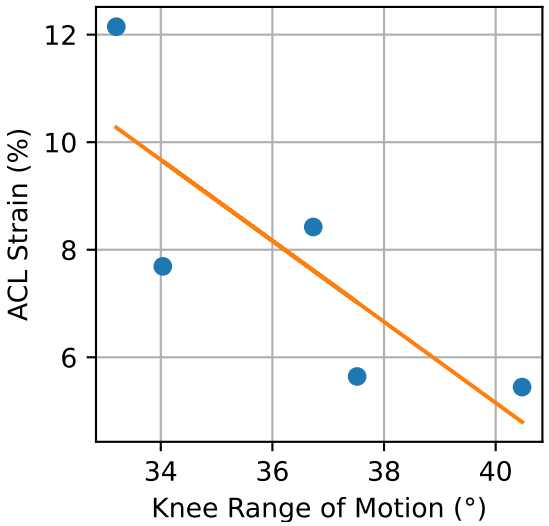

Figure 5.1: Correlation regression of knee range of flexion and ACL strain

Hip Flexion

The moderate correlation observed between hip flexion angles and ACL strain in a bivariate statistical analysis also suggests that other factors were involved as significant contributors. Yu et al. (2006) reported mean peak hip flexion angles (46±10° for females, 56±32° for males) which were close to the ones observed in this study (59±6.7°).

The hip displacement curves are shown in Figure 4.1 represent the relative rise and fall distance between the hip and the ankle node along the vertical Y-axis. The initial increase in hip Y-displacement reflects the extension of the lower limb continuing slightly past the initial ground contact time. It was interesting to note that the two male participants (P2 and P3) exhibited a noticeable continuation of leg extension well past the initial ground contact point while the remaining three female participants maintained their relative hip-to-ankle distances immediately following ground contact. The greater leg extension in P2 and P3 was also observed in the ankle displacement plot in Figure 4.2. The ankle experiences a negative displacement in the X-axis relative to the hip, as it travels forward while the foot was anchored to the ground during the landing. The two male participants exhibited the greatest negative ankle displacements despite not having the longest limb lengths.

This behavior was also reflected in Table 4.3, which shows that P2 and P3 have the

lowest peak hip flexion angles, both around 53°, compared to the three other female participants. This was found to be the opposite gender-specific result from Yu et al. (2006), where their female participants exhibited lower maximum hip flexion angles throughout the landing. The other two studies in Table 5.1 did not report hip flexion angle values. Therefore it was still unclear whether there were gender-based differences in hip flexion during stop-jump landings. However both the Yu et. al. (2006) study and the current one found no correlation between peak hip and knee flexion angles and peak GRFs, as neither of the two male participants in this study had the highest vertical GRF despite having the lowest hip flexion angles. This suggests that increased hip flexion angles alone do not necessarily lead to reduced landing impact force. An increased GRF, particularly in the posterior direction for stop-jump tasks, was found to create a greater anterior tibial shear force which translates to greater ACL strain (Kar & Quesada, 2012). Therefore seeing that there was no correlation between peak hip flexion and GRF for this study, it makes sense that there was no observed correlation between hip flexion and ACL strain either.

It was remarked however that there was a strong inverse correlation between peak hip flexion and meniscus strain. Table 4.4 shows a -0.75 Pearson coefficient, where absolute values greater than 0.7 were considered a strong association (Mukaka, 2012). In other words, as the hip was flexed more, the FE model experienced less deformation in the meniscus. Limited literature exists discussing the direct relationship between hip flexion and meniscus strain, however it was known that increased hip flexion allows for more shock absorption in the knee joint (Pollard et al., 2010). While it was recognized again that the statistical significance could be greater, it can be a reasonable hypothesis to suggest that landing with a greater hip flexion can reduce the strain experienced by the meniscus during jump landings for future studies with greater samples sizes.

The other parameters included in the bivariate correlation analysis, such as ankle flexion and trunk flexion, lacked significant correlation with both ACL and meniscus strain in the results of this study.

5.2 Muscle Force and Joint Moment Contributions

5.2.1 Validation of Kinetics

As presented in Table 4.1, the peak residual forces for all five participants were around 5% or less of the maximum external load, as recommended by the developers of *OpenSim* (J. L. Hicks et al., 2015). The peak residual moments were also less than 5% of the

maximum external moment, which was determined by multiplying the maximum vertical GRF with the vertical component of each participant's center of mass location. Residual forces and moments represent a term of "left-over" values that the *OpenSim* algorithm generates in order to achieve a force balance between external forces and the acceleration of the system. Hence low residual values were a way of validating that computed muscle force values with minimal error.

Moreover, input forces and moments in *Abaqus* have prescribed values, meaning they were entered as definitions for the FE simulation (*About Prescribed Conditions*). If *Abaqus* was unable to obey these predefined fields, the FE simulation would abort. Therefore all the output velocities, muscle forces and joint moments from the FE simulations followed the same values as the outputs from the processed *OpenSim* results.

P2 Outlier

It was recognized that the peak quadriceps forces from P2 shown in Figure 4.3 were significantly higher than the other participants. P2 also exhibited opposite directions for the internal hip and ankle moment, as seen in Figure 4.4. The other four participants exhibited either little or no internal hip flexion moment at the start of the jump and swung backwards into a hip extension moment as the landing progresses. They also exerted an internal ankle extension moment as they decelerated the landing, the magnitude of which dropped as the ankle began to plantarflex, preparing for the following take-off. Conversely, P2 experienced an internal hip flexion moment and an internal ankle flexion moment for all of the simulated landing time. The distinction between internal and external moments was that internal moments were generated by actuating muscle forces while external moments were a result of external body acceleration. Though it was not plotted, Table 4.3 also shows that P2 exerted high trunk flexion moments as well, which was often paired with hip flexion motions. One possible explanation for this outlier behavior was that the participant may have intentionally tried to land with a greater joint flexions. P2 did in fact have the highest flexion angles for both peak trial and maximum GRF instances at the knee, ankle, and trunk, but not at the hip. Therefore this participant may have been consciously trying to lean into the landing at the trunk, knee, and ankle.

The biomechanical effect of having high quadriceps forces was consistent with these internal flexion joint moments observed in P2. The quadriceps muscles, particularly the rectus femoris muscle is known to be a significant hip flexor muscle (Frigo et al., 2010). Figure 4.3 also shows that P2 had the lowest hamstrings force, which was to be expected as hamstrings are antagonist to quadriceps forces, and induce internal hip extension moments (Yanagisawa & Fukutani, 2020).

The high quadriceps forces observed in P2 made it challenging for the FE simulation to converge in *Abaqus* with the anatomical definitions of this model in particular. Therefore the elastic stiffness of the patellar tendon connectors had to be artificially increased. The stiffness was doubled to 360 N/mm for P2 only, which was the minimum stiffness needed for the simulation to complete correctly, while the remaining participants had a stiffness of 180 N/mm. To verify that this increase in patellar tendon stiffness does not significantly affect the strain values for the ACL or the meniscus, a participant whose FE simulation completed successfully with the anatomical stiffness (180 N/mm) value was also simulated separately at increased stiffness (360 N/mm). Figure 5.2 below shows the strain comparison results simulated on P1. There was almost no significant difference in neither ACL nor meniscus strain after doubling the patellar tendon stiffness. Therefore the strain values for P2 were still representative of the participant's landing biomechanics despite the stiffness increase.

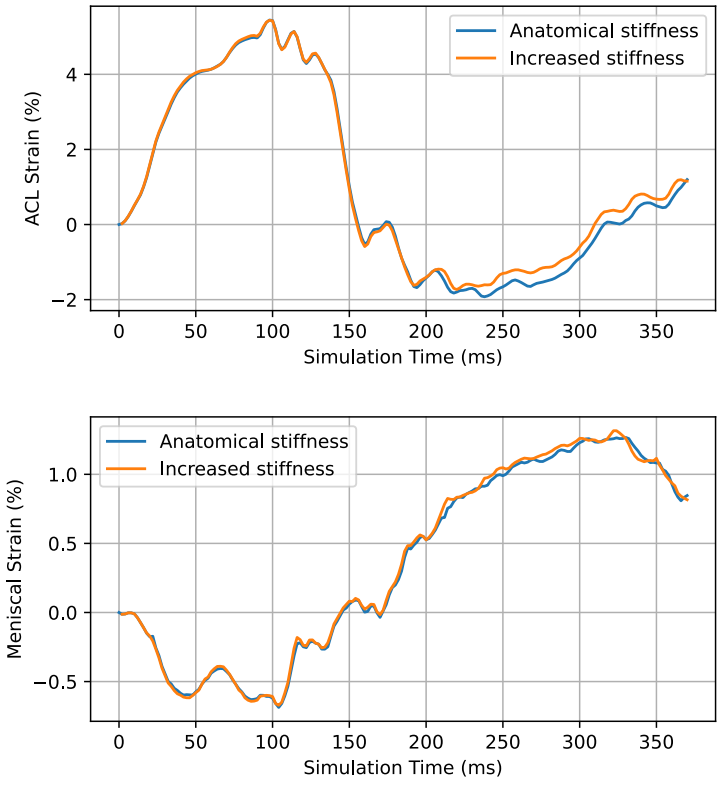

Figure 5.2: Strain outputs comparing normal to artificially increased patellar tendon stiffness for P1

5.2.2 Muscle Force and Joint Moment Correlations with Strain

If the higher quadriceps forces in P2 were disregarded, the average muscle force values found in this study were comparable to previous jump-landing studies. One study looked at the muscle force contributions towards ACL loading for two-leg stop-jump landings and found that the sum of peak quadriceps muscle forces (the vastus and rectus femoris muscles) was only 1.25 times the body mass (Peel et al., 2021). This was much lower than the average proportion found in this study, where the average quadriceps to body mass ratio was about 7 times. There were also a few other stop-jump related studies that acquired muscle force data, however they were reported in terms of relative EMG activation units such as percent of maximum contraction rather than force units (Chappell et al., 2007; Edwards et al., 2012). Another two-leg stop-jump landing study also found a much lower peak internal knee extension moment, with a mean of only 0.3 Nm/kg of body mass (Kar & Quesada, 2012). The equivalent mean peak knee extension found in this study was much greater at 3 Nm/kg of body mass. When widening the scope of comparison to vertical-jump landings, more commonality in muscle force behavior was observed. Bakker (2014) found a similar range of peak muscle forces, with an average of 3.5 kN for quadriceps, 1.3 kN for hamstrings, and 1.1 kN for calf forces. These values were lower than the mean values found in this study when comparing to the 4.7 kN for quadriceps, 2.9 kN for hamstrings, and 1.7 kN for calf forces. Another vertical-jump landing study (Walsh et al., 2012) also reported a 3.04 quadriceps to hamstrings force ratio while this study found a ratio of 4.16 if excluding P2. Therefore there is still a need for further investigation into the typical muscle force and joint moment range for stop-jump landings, particularly for single-leg landings where all of the external forces were supported by one leg rather than two.

5.3 Overall Strain Behavior

The gauge length for both ACL and meniscus strain calculations was set to the start of the linear force ramp-up phase of the simulation. The reasoning for this was visible in Figure 4.5, which shows that before the kinematic inputs become active, the ACL and meniscus strain experienced notable elastic deformation as the muscle groups and joint moments gradually began actuating while the FE knee model remained stationary. Therefore any strain observed during this period was purely a result of muscle force and joint moment inputs.

5.3.1 ACL Strain

For the ACL strains, the first behavior one may remark is that the strain decreased for most participants as the landing progressed and that the peak ACL strain occurred near the start of the landing, before the peak GRF time. Only P3 and P5 showed a notable increase in ACL strain before entering a negative strain region, at which the ACL connector was more relaxed than the tension experienced at the FE model's resting position. The two-leg stop-jump study by Kar et al. (2012) also found that their peak ACL strains occurred during the first 20% of the landings. One possible explanation for the peak strain occurring before the peak GRF instance was that once the knee joint experienced a certain degree of compression, the tibia underwent little to no further anterior translation. Therefore as the knee continued to flex during the landing, the vertical gap between the two insertion sites of the ACL ligament closed faster than the lengthening effects created by any additional tibial translation. The net decrease in distance between the two insertion sites caused the tension in the ACL to decrease, even if the GRF had yet to peak, hence exhibiting a negative strain.

The possibility that increased compression limited the anterior tibial translation, and in turn the ACL strain, was reflected in the meniscus strain behavior in Figure 4.5 as well. It can be observed that as the ACL relaxed, there was an overall upwards trend in meniscus strain, indicating increased compression in the knee.

A comparison of the strains obtained in this study between the values found in literature is summarized in Table 5.1 below. The mean peak ACL strain of 7.9% $\pm$2.4 from this study fell within a middle range when compared to a few previous ACL strain studies shown in Table 5.2. Out of the listed studies, only Kar and Quesada (2012) replicated a stop-jump experiment. The other five studies were vertical-jump landings where the participants were asked to either land from a maximal height jump or from a platform. The Cerulli (2003) study included a single participant, as it was an *in-vivo* experiment, where the participant had strain gauges surgically implanted into their ACL and asked to hop across the forceplate as quickly as possible. Although these were different types of jump maneuvers, their strain values showed that the strains observed in the current study fell within a reasonable range.

The mean 4.3% difference in ACL strain between the current study and the study by Kar and Quesada (2012) can be attributed to the many differences in landing and modeling approaches. Their two-leg study asked participants to jump from a 50 cm high platform forwards onto the forceplate and to remain in a stabilized landing pose rather than to spring back up into a second jump. Therefore the additional 50 cm height added to their stop-jump likely contributed to their higher ACL strain values. Moreover, their ACL was

modeled in *OpenSim* using a much simpler knee joint model compared to the FE model used in this study. Therefore slight differences in ACL strains are to be expected.

Table 5.2: Mean peak ACL strain values

Study	Landing-type	Strain (%)	SD
Current study	single-leg stop-jump	7.9	±2.4
Kar & Quesada (2012)	two-leg stop-jump (*OpenSim* model)	12.2	±4.1
Cerulli (2003)	hop jump (*in-vivo; strain gauge*)	5.47	±0.28
Taylor & Terry (2011)	vertical-jump (*in-vivo; MRI*)	12.0	± 7.0
Bakker et al. (2014)	vertical-jump (*in-vitro*)	10.9	-
Polak (2018)	vertical-jump (LS Dyna model)	4.4	±1.8
Rao (2020)	vertical-jump (*Abaqus* model)	5.4	±2.6

ACL Strain Regression Analysis

Bivariate correlation analysis does not easily reveal the relationship between a response and several simultaneous parameters. It was well recognized that the parameters in Table 4.3 were interrelated and can be both antagonists to each other or co-contributors towards increased strain. Therefore multivariate linear regression was also performed on the same parameters to quantify these relationships in the form of models based on the empirical data found in this study. Since computational models that can measure ACL and meniscus strain require time and effort to develop, these regression models can offer a rough estimate of the expected strain in stop-jump tasks given certain parameter values which can be obtained from more readily available biomechanics tools such as motion capture data and generic musculoskeletal models in *OpenSim*.

The ACL strain regression model with the highest statistical significance and adjusted R^2 values is presented in Table 4.5. The high R^2 value signifies that 91% of the variance was accounted for by the model. Moreover, the p-value falls within the statistical significance, which in this regression analysis corresponds to a two-tailed hypothesis test. For a one-sided lower-tailed hypothesis test, the p-value would be halved (Geyer, 1999).

The intercept constant carried the majority of the variance for the ACL strain estimation. The significance of this constant was explained by Bakker et al. (2016) as being a "knee anatomic factor", which encompassed all anatomical factors and was unique to each knee on which experiments were being conducted. This means that the ACL regression

model presented was specific to the FE knee model used in this study. This study did not focus on anatomy-specific differences in biomechanical behavior but recognized the importance of further iterations of studies to validate the application of a knee-specific constant. However, the value of presenting this ACL strain regression model was mainly to understand which sagittal plane parameters were the best candidates to make predictions on ACL strain behavior.

Section 5.1.2 discussed the reasoning behind the strong inverse correlation between increased knee range of flexion at peak GRF and decreased ACL strain. Therefore it was no surprise that this parameter contributed to the strain value with strong statistical significance (p=0.025). However, it was interesting to remark that the quadriceps forces had a negative coefficient, meaning it protected the ACL. It is postulated in many studies that high quadriceps forces lead to excessive anterior tibial translation, which causes ACL damage (Withrow et al., 2006; DeMorat et al., 2004; Fleming, Renstrom, Beynnon, et al., 2001). The proposed mechanism is that with greater posterior GRF, the quadriceps must contract more to balance out the increased external knee flexion moment during the landing. The contraction from the quadriceps needed to produce an internal knee extension moment was thought to induce anterior tibial shear, which would load the ACL (Peel et al., 2021). However, Hashemi et al. (2010) countered this theory by showing that even when quadriceps loads were applied unopposed during an *in-vitro* simulated landing, the ACL did not show signs of injury nor excessive strain. Instead, the slope of the tibial plateau was shaped such that, during moderate knee flexion angles, the tibial plateau rotated posteriorly upwards about the femur, just enough that there was a resulting posteriorly directed shear force on the tibia. At the same time, it was possible that compressive forces allowed the tibia to tightly cradle the contours of the medial femoral condyle. Therefore, at moderate to high knee flexion angles where a posterior tibial shear force was induced, greater quadriceps contraction encouraged the resistance of anterior tibial translation, and in turn excessive ACL strain.

The ACL behavior observed in this study was consistent with the explanations provided by Hashemi et al. (2010). It is visible in Figure 5.3 that the tibia was indeed angled downwards anteriorly relative to the femur, as explained by Hashemi et al. (2010). A quadriceps contraction under these conditions would result in a posterior tibial shear and add compression between the femur and the tibia. This added compression along with the angulation can prevent additional anterior sliding from the tibia. Moreover, P2 was simulated under higher than usual quadriceps forces, and yet did not exhibit the greatest ACL strain at any point along the simulation time compared to the other participants, as shown in Figure 4.5. P2 also experienced the highest compression by the meniscus as it exhibited the highest peak meniscus strain of all participants. Moreover, P2 had the

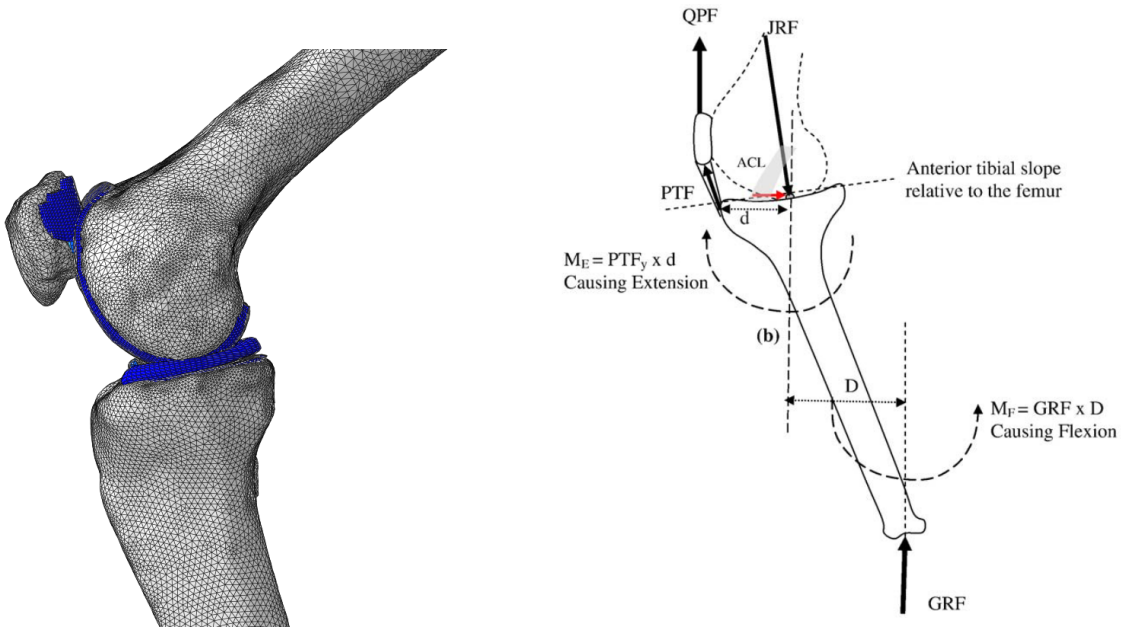

Figure 5.3: Visual representation of the tibial angulation relative to the femur in current study (left), consistent with the schematic adapted from Hashemi et al. (2010) (right).

lowest hamstring forces for the majority of the simulated landing, meaning the effects of their high quadriceps forces were even less opposed. Although there were no GRFs applied directly in these simulations, the velocity inputs applied at the hip and ankle node created an equivalent effect, where the acceleration of the hip and ankle created an external flexion moment on the knee during the simulated landing.

Therefore the ACL strain regression model presented not only offered a predictive model for the knee anatomy used in this study, but also highlighted the interrelated behavior between knee range of flexion, quadriceps forces, and ACL strain. The findings helped dispel the well-cited notion that high quadriceps forces are damaging to the ACL. The observations also served to clarify that simply having high knee flexion angles during landing does not necessarily translate to reduced ACL strain, but rather landing with a high knee range of flexion. The results showed that this combination of higher quadriceps forces paired with a large range of additional post-contact knee flexion was a significant contributor towards decreasing the risk of ACL injury.

5.3.2 Meniscus Strain

The meniscus strain behavior for all five participants generally followed a trend of relaxing during the forces and moments ramp-up period, followed by an increase in strain. An overall subsequent drop in meniscus strain occurring at different times for each participant corresponded to the time which the participant had reached maximum knee flexion and was beginning to rise back up into the second jump.

Average peak compressive meniscus strain values (1.01% ±0.65) were similar to an *in-vitro* study by Kolaczek et al. (2016), who obtained average strain values of 2.2% from 10 cadaver specimens being loaded by cables representing quadriceps and hamstring forces. Their measurement location was also the posterior side of the medial meniscus, however they used Teflon markers which were visualized with computed tomography (CT) imaging. Therefore the small strain differences can be attributed to the significant differences in experimental methods. Rao (2020) also measured meniscus strain and obtained an average peak strain of 2.3% ±1.6 for vertical-jump landings. It was very likely that meniscus strains from vertical-jump landings were slightly higher than a stop-jump landing as there was greater vertical GRF in a vertical-jump landing and greater overall landing impact.

Meniscus Strain Regression Analysis

The regression model with both the greatest adjusted R^2 and the lowest p-value is also presented for the meniscus strain. This model included a single parameter because a statistically significant model including two parameters could not be computed from the current data. Hence the knee extension moment at the peak GRF instance were the best candidate as a meniscus strain behavior predictor. With a Pearson correlation coefficient of 0.796 (p=0.025), increasing the knee extension moment at peak GRF was found to be strongly correlated with higher meniscus strain. This relationship likely arose from the compressive forces generated during the landing as the participant decelerated the landing and prepared for the second jump. A greater pressure applied to the meniscus during a high knee extension moments would cause greater deformations in the cartilage, leading to higher risk of tearing. Further iterations of studies would help further quantify the relationship between knee extension at peak GRF and meniscus deformation. However, one can suggest from the data that activities involving high knee extensions should be avoided to prevent meniscus injury, particularly if there is a history of ACL injury. Since osteoarthritis is a prevalent condition among those with ACL and meniscus damage (Hall et al., 2016), injuring both would significantly increase the risks of developing this degenerative disease.

5.4 Limitations and Future Works

It was recognized that there were a few limitations in this study that should be remarked. Some of the main limitations and associated recommendations for future works are included below:

1. The greatest limitation of this study would most likely be the small sample size of participants. This made it challenging to evaluate correlations between the sagittal plane parameters and strain values with a high level of statistical certainty. Comparisons with literature findings were relied upon to complement relationships with strong correlation coefficients but with p-values that did not pass the statistical significance threshold. The inclusion of 10-15 participants for future iterations or variations of this study is recommended for a clearer statistical analysis of the strain behavior relationships.

2. This study was among the first to study the ACL and meniscus strain using an FE model for a stop-jump task. Although this was what made this study novel, the lack of equivalent experimental results put limitations on how much validation can be done on the computational models used in this study. Although the FE model itself was thoroughly validated by Rao (2020) for vertical-jump landings, there had yet to be *in-vitro* experimental data which could confirm the range of values obtained in this study. While this study provided a powerful predictive model, it is recommended to have follow-up experiments which would include ACL and meniscus strain measurement, using either EMG data that can be compared with Newton and torque units, or using a DKS.

3. Although this study did not focus on the FE knee model building process, it was recognized that certain definitions of the FE model were simplified and grouped. For instance, the soleus muscle was found to have significant activation throughout the landings, however it was grouped with other plantar flexor muscles and modeled as a torque rather than a muscle fibre actuator. While the net torque contribution created by the soleus muscle was accounted for, this approach may be simplified and mask potential biomechanically meaningful observations that were valuable to model computationally. Due to the debated nature of quadriceps force contributions towards increased ACL strain, it may also be beneficial to model each of the four main quadriceps muscles muscle individually and investigate further how each component induces a posterior-directed tibial shear force.

Chapter 6

Conclusion

6.1 Summary

The objective of this study was to understand the significant sagittal plane parameters that contributed to increased risk of ACL and meniscus strain. A computational approach was taken using biomechanical modeling capabilities from *OpenSim* and the anatomically representative FE model in *Abaqus*. With the existing force plate and motion capture data for stop-jump landings, *OpenSim* offered the ability to compile the kinematics from the motion capture data, and compute muscle force values that were consistent with the applied GRF for each individual participant. The kinematics, muscle forces and joint moments were then applied to an FE model, which allowed for inputs to be simulated on a more accurate geometrical and material definition of the knee joint than what was possible in *OpenSim*. The ACL and meniscus strain results from the simulation were then compared to the main sagittal plane parameters in a bivariate correlation comparison, with the best candidates fitted to a multivariate linear regression model.

Both the kinematic and kinetic outputs from *OpenSim* were verified by computing the peak residual forces, moments and both rotational and translational pErrors. Values for peak knee flexion angle were also compared with other two-leg stop-jump landings studies were found to fall within the middle of the range, confirming that the FE model produced reasonable strain-values for this type of landing. Although there was a moderate correlation between increased ACL strain and peak knee flexion (r=-0.51, p=0.43), it was observed that the knee range of flexion was in fact a better predictor for the risk of ACL damage (r=-0.81, p=0.075). The results indicated that a distinction should be emphasized between the peak knee flexion of the landing and the knee range of flexion, as the knee

range of flexion better characterizes a "soft-landing" and provides more relief for the ACL. Another remark from the regression analysis for the ACL was that the quadriceps forces did not increase the risk of excessive tibial translation. Contrary to what was commonly cited in literature, no correlation between high quadriceps forces and increased ACL strain was observed. It was seen in the FE simulation results that the angulation of the tibia relative to the femur actually results in a posterior tibial shear, which in turn protects the ACL by resisting anterior translation. The meniscus was found to have an average peak strain of 1.01%±0.65, which fell within a close range to the limited number of other studies which have been able to measure meniscus strain. It was observed that high internal knee extension moments were correlated with increased meniscus strain, which was likely attributed to the high compressive forces applied to the meniscus while the participant was attempting to decelerate the landing.

The findings of this thesis have strengthened the conclusions of previous studies as well as introduced a new approach to studying the ACL and meniscus. Focusing on the importance of increasing flexion over the landing's period of time rather than instantaneous flexion angles provided a more representative and holistic understanding of how to avoid over-straining the knee joint. This behavior combined with strengthening the quadriceps muscles can reduce the risk of excessive anterior tibial translation. Detailed quantification of these results was made possible by simulating the motion on an FE knee model. One of the greatest challenges in biomechanics studies is visualizing and applying measurements to anatomical components that are embedded as deep inside the knee joint as the ACL and meniscus. With the computational approach executed in this study, one can promote well-informed, effective, and safe landing practices.

References

About Prescribed Conditions. (n.d.). Retrieved 2021-07-07, from https://abaqus-docs.mit.edu/2017/English/SIMACAEPRCRefMap/simaprc-c-prescribedover.htm

Akoglu, H. (2018, August). User's guide to correlation coefficients. *Turkish Journal of Emergency Medicine*, *18*(3), 91–93. Retrieved 2021-07-04, from https://www.ncbi.nlm.nih.gov/pmc/articles/PMC6107969/ doi: 10.1016/j.tjem.2018.08.001

Bakker, R. (2014). *The Effect of Sagittal Plane Mechanics on Anterior Cruciate Ligament Strain During Jump Landing* (Unpublished master's thesis). University of Waterloo, Waterloo.

Bakker, R., Tomescu, S., Brenneman, E., Hangalur, G., Laing, A., & Chandrashekar, N. (2016). Effect of sagittal plane mechanics on ACL strain during jump landing. *Journal of Orthopaedic Research*, *34*(9), 1636–1644. Retrieved 2021-04-03, from https://onlinelibrary.wiley.com/doi/abs/10.1002/jor.23164 (_eprint: https://onlinelibrary.wiley.com/doi/pdf/10.1002/jor.23164) doi: https://doi.org/10.1002/jor.23164

Becker, J., Emmanuel, M., & Jean-Marc, L. (2019, July). Joint Loading Estimation Method for Horse Forelimb High Jerk Locomotion: Jumping. *Journal of Bionic Engineering*, *16*(4), 674–685. Retrieved 2021-07-22, from https://doi.org/10.1007/s42235-019-0054-z doi: 10.1007/s42235-019-0054-z

Blackburn, J. T., & Padua, D. A. (2008, March). Influence of trunk flexion on hip and knee joint kinematics during a controlled drop landing. *Clinical Biomechanics (Bristol, Avon)*, *23*(3), 313–319. doi: 10.1016/j.clinbiomech.2007.10.003

Blankevoort, L., Kuiper, J. H., Huiskes, R., & Grootenboer, H. J. (1991). Articular contact in a three-dimensional model of the knee. *Journal of Biomechanics*, *24*(11), 1019–1031. doi: 10.1016/0021-9290(91)90019-j

Brekelmans, W. A. M., Poort, H. W., & Slooff, T. J. J. H. (1972, January). A New Method to Analyse the Mechanical Behaviour of Skeletal Parts. *Acta Orthopaedica Scandinavica*, *43*(5), 301–317. Retrieved 2021-07-22, from https://doi.org/10.3109/17453677208998949 (Publisher: Taylor & Francis _eprint: https://doi.org/10.3109/17453677208998949) doi: 10.3109/17453677208998949

Cassidy, K. (2009). *Design and Development of a Dynamic Knee Injury Simulator* (Doctoral dissertation, University of Waterloo). Retrieved 2021-07-15, from https://uwspace.uwaterloo.ca/handle/10012/4683 (Accepted: 2009-09-02T20:50:51Z Publisher: University of Waterloo)

Cerulli, G., Benoit, D. L., Lamontagne, M., Caraffa, A., & Liti, A. (2003, September). In vivo anterior cruciate ligament strain behaviour during a rapid deceleration move-

ment: case report. *Knee surgery, sports traumatology, arthroscopy: official journal of the ESSKA*, *11*(5), 307–311. doi: 10.1007/s00167-003-0403-6

Chandrashekar, N., Mansouri, H., Slauterbeck, J., & Hashemi, J. (2006). Sex-based differences in the tensile properties of the human anterior cruciate ligament. *Journal of Biomechanics*, *39*(16), 2943–2950. doi: 10.1016/j.jbiomech.2005.10.031

Chandrashekar, N., Slauterbeck, J., & Hashemi, J. (2005, October). Sex-based differences in the anthropometric characteristics of the anterior cruciate ligament and its relation to intercondylar notch geometry: a cadaveric study. *The American Journal of Sports Medicine*, *33*(10), 1492–1498. doi: 10.1177/0363546504274149

Chappell, J. D., Creighton, R. A., Giuliani, C., Yu, B., & Garrett, W. E. (2007, February). Kinematics and Electromyography of Landing Preparation in Vertical Stop-Jump: Risks for Noncontact Anterior Cruciate Ligament Injury. *The American Journal of Sports Medicine*, *35*(2), 235–241. Retrieved 2021-07-09, from https://doi.org/10.1177/0363546506294077 (Publisher: SAGE Publications Inc STM) doi: 10.1177/0363546506294077

Dahiru, T. (2008, June). P-Value, a True Test of Statistical Significance? A Cautionary Note. *Annals of Ibadan Postgraduate Medicine*, *6*(1), 21–26. Retrieved 2021-07-06, from https://www.ncbi.nlm.nih.gov/pmc/articles/PMC4111019/

Dai, B., Garrett, W. E., Gross, M. T., Padua, D. A., Queen, R. M., & Yu, B. (2019, May). The effect of performance demands on lower extremity biomechanics during landing and cutting tasks. *Journal of Sport and Health Science*, *8*(3), 228–234. Retrieved 2021-07-04, from https://www.sciencedirect.com/science/article/pii/S2095254616301016 doi: 10.1016/j.jshs.2016.11.004

Dai, B., Sorensen, C. J., Derrick, T. R., & Gillette, J. C. (2012, December). The Effects of Postseason Break on Knee Biomechanics and Lower Extremity EMG in a Stop-Jump Task: Implications for ACL Injury. *Journal of Applied Biomechanics*, *28*(6), 708–717. Retrieved 2021-07-20, from https://journals.humankinetics.com/view/journals/jab/28/6/article-p708.xml (Publisher: Human Kinetics, Inc. Section: Journal of Applied Biomechanics) doi: 10.1123/jab.28.6.708

Decker, M. J., Torry, M. R., Wyland, D. J., Sterett, W. I., & Richard Steadman, J. (2003, August). Gender differences in lower extremity kinematics, kinetics and energy absorption during landing. *Clinical Biomechanics (Bristol, Avon)*, *18*(7), 662–669. doi: 10.1016/s0268-0033(03)00090-1

Delp, S. L., Anderson, F. C., Arnold, A. S., Loan, P., Habib, A., John, C. T., ... Thelen, D. G. (2007, November). OpenSim: Open-Source Software to Create and Analyze Dynamic Simulations of Movement. *IEEE Transactions on Biomedical Engineering*, *54*(11), 1940–1950. (Conference Name: IEEE Transactions on Biomedical Engineering) doi: 10.1109/TBME.2007.901024

DeMorat, G., Weinhold, P., Blackburn, T., Chudik, S., & Garrett, W. (2004, March). Aggressive quadriceps loading can induce noncontact anterior cruciate ligament injury. *The American Journal of Sports Medicine*, *32*(2), 477–483. doi: 10.1177/0363546503258928

Edwards, S., Steele, J. R., Cook, J. L., Purdam, C. R., & McGHEE, D. E. (2012, June). Lower Limb Movement Symmetry Cannot Be Assumed When Investigating the Stop–Jump Landing. *Medicine & Science in Sports & Exercise*, *44*(6), 1123–1130. Retrieved 2021-07-09, from https://journals.lww.com/acsm-msse/Fulltext/2012/06000/Lower_Limb_Movement_Symmetry_Cannot_Be_Assumed.20.aspx doi: 10.1249/MSS.0b013e31824299c3

Elias, J. J., Faust, A. F., Chu, Y.-H., Chao, E. Y., & Cosgarea, A. J. (2003, March). The Soleus Muscle Acts as an Agonist for the Anterior Cruciate Ligament: An in Vitro Experimental Study. *The American Journal of Sports Medicine*, *31*(2), 241–246. Retrieved 2021-07-15, from https://doi.org/10.1177/03635465030310021401 (Publisher: SAGE Publications Inc STM) doi: 10.1177/03635465030310021401

Fernández-Moreno, M., Rego, I., Carreira-Garcia, V., & Blanco, F. J. (2008, December). Genetics in Osteoarthritis. *Current Genomics*, *9*(8), 542–547. Retrieved 2021-07-12, from https://www.ncbi.nlm.nih.gov/pmc/articles/PMC2694558/ doi: 10.2174/138920208786847953

Filho, D. B., Paranhos, R., Rocha, E. C. d., Batista, M., Silva Jr., J. A. d., Santos, M. L. W. D., & Marino, J. G. (2013). When is statistical significance not significant? *Brazilian Political Science Review*, *7*, 31–55. Retrieved 2021-07-04, from https://www.scielo.br/j/bpsr/a/DhwrWkLLkhHVbdgTZGtMqyD/abstract/?lang=en (Publisher: Associação Brasileira de Ciência Política)

Fleming, B. C., Renstrom, P. A., Beynnon, B. D., Engstrom, B., Peura, G. D., Badger, G. J., & Johnson, R. J. (2001, February). The effect of weightbearing and external loading on anterior cruciate ligament strain. *Journal of Biomechanics*, *34*(2), 163–170. doi: 10.1016/s0021-9290(00)00154-8

Fleming, B. C., Renstrom, P. A., Ohlen, G., Johnson, R. J., Peura, G. D., Beynnon, B. D., & Badger, G. J. (2001). The gastrocnemius muscle is an antagonist of the anterior cruciate ligament. *Journal of Orthopaedic Research*, *19*(6), 1178–1184. Retrieved 2021-07-11, from https://onlinelibrary.wiley.com/doi/abs/10.1016/S0736-0266%2801%2900057-2 (_eprint: https://onlinelibrary.wiley.com/doi/pdf/10.1016/S0736-0266%2801%2900057-2) doi: 10.1016/S0736-0266(01)00057-2

Frigo, C., Pavan, E. E., & Brunner, R. (2010, January). A dynamic model of quadriceps and hamstrings function. *Gait & Posture*, *31*(1), 100–103. Retrieved 2021-07-07,

from https://www.sciencedirect.com/science/article/pii/S0966636209006195 doi: 10.1016/j.gaitpost.2009.09.006

Gayzik, F. S., Moreno, D. P., Geer, C. P., Wuertzer, S. D., Martin, R. S., & Stitzel, J. D. (2011, October). Development of a full body CAD dataset for computational modeling: a multi-modality approach. *Annals of Biomedical Engineering*, *39*(10), 2568–2583. doi: 10.1007/s10439-011-0359-5

Getting Started with Scaling - OpenSim Documentation - Global Site. (n.d.). Retrieved 2021-07-21, from https://simtk-confluence.stanford.edu/display/OpenSim/Getting+Started+with+Scaling

Geyer, C. (1999). *Simple Linear Regression in Rweb.* Retrieved 2021-07-11, from http://users.stat.umn.edu/~geyer/classes/3011/rweb/rsimp.html

Godest, A. C., Beaugonin, M., Haug, E., Taylor, M., & Gregson, P. J. (2002, February). Simulation of a knee joint replacement during a gait cycle using explicit finite element analysis. *Journal of Biomechanics*, *35*(2), 267–275. doi: 10.1016/s0021-9290(01)00179-8

Gomes, J. L. E., de Castro, J. V., & Becker, R. (2008, September). Decreased hip range of motion and noncontact injuries of the anterior cruciate ligament. *Arthroscopy: The Journal of Arthroscopic & Related Surgery: Official Publication of the Arthroscopy Association of North America and the International Arthroscopy Association*, *24*(9), 1034–1037. doi: 10.1016/j.arthro.2008.05.012

Griffin, L. Y., Albohm, M. J., Arendt, E. A., Bahr, R., Beynnon, B. D., Demaio, M., ... Yu, B. (2006, September). Understanding and preventing noncontact anterior cruciate ligament injuries: a review of the Hunt Valley II meeting, January 2005. *The American Journal of Sports Medicine*, *34*(9), 1512–1532. doi: 10.1177/0363546506286866

Guo, Y., Zhang, X., & Chen, W. (2009, August). Three-dimensional Finite Element Simulation of Total Knee Joint in Gait Cycle. *Acta Mechanica Solida Sinica*, *22*(4), 347–351. Retrieved 2021-07-22, from https://doi.org/10.1016/S0894-9166(09)60283-4 doi: 10.1016/S0894-9166(09)60283-4

Hall, M., Bryant, A. L., Wrigley, T. V., Pratt, C., Crossley, K. M., Whitehead, T. S., ... Perraton, L. G. (2016, May). Does meniscal pathology alter gait knee biomechanics and strength post-ACL reconstruction? *Knee Surgery, Sports Traumatology, Arthroscopy*, *24*(5), 1501–1509. Retrieved 2021-07-12, from http://link.springer.com/10.1007/s00167-015-3908-x doi: 10.1007/s00167-015-3908-x

Hamner, S. R., Seth, A., & Delp, S. L. (2010, October). Muscle contributions to propulsion and support during running. *Journal of Biomechanics*, *43*(14), 2709–2716. doi: 10.1016/j.jbiomech.2010.06.025

Hashemi, J., Breighner, R., Jang, T.-H., Chandrashekar, N., Ekwaro-Osire, S., & Slauterbeck, J. R. (2010, June). Increasing pre-activation of the quadriceps muscle pro-

tects the anterior cruciate ligament during the landing phase of a jump: An in vitro simulation. *The Knee*, *17*(3), 235–241. Retrieved 2021-07-11, from https://www.sciencedirect.com/science/article/pii/S096801600900177X doi: 10.1016/j.knee.2009.09.010

Hicks, J. (2018). *CMC Best Practices - OpenSim 3.3 Documentation.* Retrieved 2021-04-03, from https://simtk-confluence.stanford.edu:8443/display/OpenSim33/_CMC+Best+Practices

Hicks, J. L., Uchida, T. K., Seth, A., Rajagopal, A., & Delp, S. L. (2015, February). Is My Model Good Enough? Best Practices for Verification and Validation of Musculoskeletal Models and Simulations of Movement. *Journal of Biomechanical Engineering*, *137*(2), 0209051–02090524. Retrieved 2021-07-07, from https://www.ncbi.nlm.nih.gov/pmc/articles/PMC4321112/ doi: 10.1115/1.4029304

Howell, D. (2015). *Randomization test on correlation coefficients.* Retrieved 2021-04-17, from https://www.uvm.edu/~statdhtx/StatPages/Randomization%20Tests/RandomCorr/randomization_Correlation.html

Kar, J., & Quesada, P. M. (2012, August). A numerical simulation approach to studying anterior cruciate ligament strains and internal forces among young recreational women performing valgus inducing stop-jump activities. *Annals of Biomedical Engineering*, *40*(8), 1679–1691. doi: 10.1007/s10439-012-0572-x

Kean, C. O., Brown, R. J., & Chapman, J. (2017, November). The role of biomaterials in the treatment of meniscal tears. *PeerJ*, *5*, e4076. Retrieved 2021-08-25, from https://peerj.com/articles/4076 (Publisher: PeerJ Inc.) doi: 10.7717/peerj.4076

Khuvasanont, T. (2002). *Age-Related Ankle Strength Degradation and Effects on Slip-Induced Falls* (Thesis, Virginia Tech). Retrieved 2021-07-22, from https://vtechworks.lib.vt.edu/handle/10919/34254 (Accepted: 2014-03-14T20:42:13Z)

Kiapour, A., Kiapour, A. M., Kaul, V., Quatman, C. E., Wordeman, S. C., Hewett, T. E., ... Goel, V. K. (2014, January). Finite Element Model of the Knee for Investigation of Injury Mechanisms: Development and Validation. *Journal of Biomechanical Engineering*, *136*(1), 0110021–01100214. Retrieved 2021-07-22, from https://www.ncbi.nlm.nih.gov/pmc/articles/PMC5101024/ doi: 10.1115/1.4025692

Kiapour, A. M., Quatman, C. E., Goel, V. K., Wordeman, S. C., Hewett, T. E., & Demetropoulos, C. K. (2014, January). Timing sequence of multi-planar knee kinematics revealed by physiologic cadaveric simulation of landing: Implications for ACL injury mechanism. *Clinical Biomechanics*, *29*(1), 75–82. Retrieved 2021-07-15, from https://www.sciencedirect.com/science/article/pii/S0268003313002362 doi: 10.1016/j.clinbiomech.2013.10.017

Kim, J. H., & Choi, I. (2019). Choosing the Level of Significance: A Decision-theoretic Approach. *Abacus*, *57*(1). doi: 10.1111/abac.12172

Kolaczek, S., Hewison, C., Caterine, S., Ragbar, M. X., Getgood, A., & Gordon, K. D. (2016, October). Analysis of 3D strain in the human medial meniscus. *Journal of the Mechanical Behavior of Biomedical Materials*, *63*, 470–475. Retrieved 2021-07-12, from https://www.sciencedirect.com/science/article/pii/S1751616116301679 doi: 10.1016/j.jmbbm.2016.06.001

Krosshaug, T., Nakamae, A., Boden, B. P., Engebretsen, L., Smith, G., Slauterbeck, J. R., ... Bahr, R. (2007, March). Mechanisms of Anterior Cruciate Ligament Injury in Basketball: Video Analysis of 39 Cases. *The American Journal of Sports Medicine*, *35*(3), 359–367. Retrieved 2021-07-18, from https://doi.org/10.1177/0363546506293899 (Publisher: SAGE Publications Inc STM) doi: 10.1177/0363546506293899

Lacey, M. (1997). *Tests of Significance.* Retrieved 2021-07-06, from http://www.stat.yale.edu/Courses/1997-98/101/sigtest.htm

Leppänen, M., Pasanen, K., Krosshaug, T., Kannus, P., Vasankari, T., Kujala, U. M., ... Parkkari, J. (2017, December). Sagittal Plane Hip, Knee, and Ankle Biomechanics and the Risk of Anterior Cruciate Ligament Injury: A Prospective Study. *Orthopaedic Journal of Sports Medicine*, *5*(12), 2325967117745487. Retrieved 2021-07-04, from https://www.ncbi.nlm.nih.gov/pmc/articles/PMC5753918/ doi: 10.1177/2325967117745487

Li, S., Luo, X., Tang, Y., Lan, H., & Yu, H. (2019, July). Simulation of Tibialis Anterior Muscle Transfer for Congenital Clubfoot Based on OpenSim. In *2019 4th Asia-Pacific Conference on Intelligent Robot Systems (ACIRS)* (pp. 39–43). doi: 10.1109/ACIRS.2019.8935979

Management of high hamstring tendinopathies — a conservative versus injection therapy approach. (2018, June). Retrieved 2021-08-25, from https://www.sportsinjurybulletin.com/management-of-high-hamstring-tendinopathies-a-conservative-versus-injection-therapy-approach/

Manal, K. T., & Buchanan, T. S. (2004). *Standard Handbook of Biomedical Engineering and Design.* University of Delaware, Newark: McGraw-Hill. Retrieved from https://web.unhas.ac.id/tahir/BAHAN-KULIAH/BIO-MEDICAL/NEW/HANBOOK/0071449337_ar005-Biomechanics_Of_Human_Movement.pdf

McLean, S. G., Oh, Y. K., Palmer, M. L., Lucey, S. M., Lucarelli, D. G., Ashton-Miller, J. A., & Wojtys, E. M. (2011, July). The Relationship Between Anterior Tibial Acceleration, Tibial Slope, and ACL Strain During a Simulated Jump Landing Task. *The Journal of Bone and Joint Surgery. American Volume*, *93*(14), 1310. Retrieved 2021-07-15, from https://www.ncbi.nlm.nih.gov/pmc/articles/PMC6882530/ (Publisher: Wolters Kluwer Health) doi: 10.2106/JBJS.J.00259

Minitab. (2019). *Model reduction* [mtbconcept]. Retrieved 2021-04-17, from

https://support.minitab.com/en-us/minitab-express/1/help-and-how-to/modeling-statistics/regression/supporting-topics/regression-models/model-reduction/

Moore, K., & Dalley, A. (1999). *Clinical Oriented Anatomy* (4th ed.). Lippincott Williams and Wilkins.

Mukaka, M. (2012, September). A guide to appropriate use of Correlation coefficient in medical research. *Malawi Medical Journal : The Journal of Medical Association of Malawi*, *24*(3), 69–71. Retrieved 2021-07-04, from https://www.ncbi.nlm.nih.gov/pmc/articles/PMC3576830/

Noyes, F. R. (2009, January). The function of the human anterior cruciate ligament and analysis of single- and double-bundle graft reconstructions. *Sports Health*, *1*(1), 66–75. doi: 10.1177/1941738108326980

Overview of the OpenSim Workflow - OpenSim 3.3 Documentation -. (n.d.). Retrieved 2021-07-21, from https://simtk-confluence.stanford.edu/display/OpenSim33/Overview+of+the+OpenSim+Workflow

Pauly, H. M., & Haut Donahue, T. L. (2015, January). 16 - Bone–meniscus interface. In S. P. Nukavarapu, J. W. Freeman, & C. T. Laurencin (Eds.), *Regenerative Engineering of Musculoskeletal Tissues and Interfaces* (pp. 377–407). Woodhead Publishing. Retrieved 2021-07-22, from https://www.sciencedirect.com/science/article/pii/B9781782423010000161 doi: 10.1016/B978-1-78242-301-0.00016-1

Peebles, A. T., Dickerson, L. C., Renner, K. E., & Queen, R. M. (2020, May). Sex-based differences in landing mechanics vary between the drop vertical jump and stop jump. *Journal of Biomechanics*, *105*, 109818. Retrieved 2021-07-18, from https://www.sciencedirect.com/science/article/pii/S0021929020302384 doi: 10.1016/j.jbiomech.2020.109818

Peel, S. A., Schroeder, L. E., & Weinhandl, J. T. (2021, May). Lower extremity muscle contributions to ACL loading during a stop-jump task. *Journal of Biomechanics*, *121*, 110426. Retrieved 2021-07-09, from https://www.sciencedirect.com/science/article/pii/S0021929021002062 doi: 10.1016/j.jbiomech.2021.110426

Polak, A. (2018). *ACL Strain During Single-Leg Jump Landing: An Experimental and Computational Investigation* (Unpublished master's thesis). University of Waterloo, Waterloo.

Pollard, C. D., Sigward, S. M., & Powers, C. M. (2010, February). Limited hip and knee flexion during landing is associated with increased frontal plane knee motion and moments. *Clinical Biomechanics*, *25*(2), 142–146. Retrieved 2021-07-04, from https://linkinghub.elsevier.com/retrieve/pii/S0268003309002447 doi: 10.1016/j.clinbiomech.2009.10.005

Pontaga, I. (2004, January). Hip and knee flexors and extensors balance in dependence on the velocity of movements. *Biology of Sport*, *21*.

Quadriceps Muscle Strain Causes, Treatment & Others Facts. (2019, July). Retrieved 2021-08-25, from https://www.healthguideline.net/2019/07/quadriceps-muscle-strain-and-treatment.html

Rao, H. (2020). *Computational Modelling of Knee Tissue Mechanics During Single-Leg Jump Landing* (Unpublished master's thesis). University of Waterloo, Waterloo.

Roy, N., Boudreau, N., Vezina, F., Tousignant, M., & Gaudreault, N. (2015, August). Comparison of knee kinematics between meniscal tear and normal control during a step-down task. *Clinical Biomechanics (Bristol, Avon)*, *30*(7), 762–764. doi: 10.1016/j.clinbiomech.2015.05.012

RRA Best Practices. (n.d.). Retrieved 2021-04-07, from https://simtk-confluence.stanford.edu/display/OpenSim/_RRA+Best+Practices

Schwartz, D., Guleyupoglu, B., Koya, B., Stitzel, J. D., & Gayzik, F. S. (2015). Development of a computationally efficient full human body finite element model. *Traffic Injury Prevention*, *16 Suppl 1*, S49–56. doi: 10.1080/15389588.2015.1021418

Sherman, M. A., Seth, A., & Delp, S. L. (2013, August). What is a Moment Arm? Calculating Muscle Effectiveness in Biomechanical Models Using Generalized Coordinates. *Proceedings of the ... ASME Design Engineering Technical Conferences. ASME Design Engineering Technical Conferences*, *2013*. Retrieved 2021-04-10, from https://www.ncbi.nlm.nih.gov/pmc/articles/PMC4404026/ doi: 10.1115/DETC2013-13633

Taylor, K., Terry, M., Utturkar, G., Spritzer, C., Queen, R., Irribarra, L., ... DeFrate, L. (2011, February). Measurement of in vivo anterior cruciate ligament strain during dynamic jump landing. *Journal of biomechanics*, *44*(3), 365–371. Retrieved 2021-07-11, from https://www.ncbi.nlm.nih.gov/pmc/articles/PMC3053134/ doi: 10.1016/j.jbiomech.2010.10.028

Understanding Gastrocnemius Muscle Tear. (2019). Retrieved 2021-08-25, from https://www.fairview.org/Patient-Education/Articles/English/u/n/d/e/r/Understanding_Gastrocnemius_Muscle_Tear_90611

Walsh, M., Boling, M. C., McGrath, M., Blackburn, J. T., & Padua, D. A. (2012, July). Lower Extremity Muscle Activation and Knee Flexion During a Jump-Landing Task. *Journal of Athletic Training*, *47*(4), 406–413. Retrieved 2021-07-09, from https://doi.org/10.4085/1062-6050-47.4.17 doi: 10.4085/1062-6050-47.4.17

Withrow, T. J., Huston, L. J., Wojtys, E. M., & Ashton-Miller, J. A. (2006, February). The relationship between quadriceps muscle force, knee flexion, and anterior cruciate ligament strain in an in vitro simulated jump landing. *The American Journal of Sports Medicine*, *34*(2), 269–274. doi: 10.1177/0363546505280906

Yanagisawa, O., & Fukutani, A. (2020, March). Muscle Recruitment Pattern of the Hamstring Muscles in Hip Extension and Knee Flexion Exercises. *Journal of Human Ki-*

netics, *72*, 51–59. Retrieved 2021-07-07, from https://www.ncbi.nlm.nih.gov/pmc/articles/PMC7126262/ doi: 10.2478/hukin-2019-0124

Yu, B., Lin, C.-F., & Garrett, W. E. (2006, March). Lower extremity biomechanics during the landing of a stop-jump task. *Clinical Biomechanics (Bristol, Avon)*, *21*(3), 297–305. doi: 10.1016/j.clinbiomech.2005.11.003